1983

The hydrogenolysis of isobutane on iridium

Rudolph Francis Klima
Iowa State University

Klima, Rudolph Francis

THE HYDROGENOLYSIS OF ISOBUTANE ON IRIDIUM

Iowa State University PH.D. 1983

The hydrogenolysis of isobutane on iridium

by

Rudolph Francis Klima

A Dissertation Submitted to the

Graduate Faculty in Partial Fulfillment of the

Requirements for the Degree of

DOCTOR OF PHILOSOPHY

Major: Chemistry

Approved:

Signature was redacted for privacy.

In Charge of Major Work

Signature was redacted for privacy.

For the Major Department

Signature was redacted for privacy.

For the Graduate College

Iowa State University
Ames, Iowa

1983

TABLE OF CONTENTS

INTRODUCTION

Hydrogenolysis reactions have been studied for many years. These reactions involve the scission of carbon-carbon bonds and the formation of hydrogen-carbon bonds. The hydrogenolysis reaction is exothermic and catalyzed by most transition elements. Hydrogenolysis catalysts are mainly employed in the reforming industry in the form of bifunctional metal acid oxide catalysts. These catalysts are mainly used in fixed bed reactors and usually catalyze dehydrogenation and isomerization as well as hydrogenolysis.

Hydrogenolysis must be accompanied by hydrocarbon adsorption via free radical type surface intermediates. Therefore, hydrogenolysis is directly related to the electronic properties of the metals used as catalysts. Some investigators have postulated hydrogenolysis to be rate limited by carbon-carbon bond scission, while others feel that adsorption of the hydrocarbon is the rate limiting step. Single crystal, polycrystalline film and supported catalysts have been employed in hydrogenolysis studies. These studies have been conducted in flow reactor systems, as well as static reaction systems, however most studies have been limited to a narrow range of pressure determined by the system used. In the following section, some of the important aspects of hydrogenolysis will be discussed and the research objectives of this thesis will be outlined.

LITERATURE REVIEW

Industrial Applications

Hydrogenolysis catalysts are important to many industrial processes. Natural gas production can be accomplished via the breakdown of large hydrocarbons into methane, ethane, propane and butane. Cracking consists of severing carbon-carbon bonds in high molecular weight hydrocarbons to produce low molecular weight hydrocarbons. Cracking also consists of isomerization of straight to branched chain hydrocarbons. Petroleum is composed of saturated straight chain, branched chain and saturated cyclic compounds -- "naphthenes" (1-8).

In the reforming process, low octane petroleum fractions boiling in the general range of gasoline are converted to compounds with higher octane numbers. Three main reactions are employed in this process: dehydrocyclization of aliphatics to aromatics, dehydrogenation of naphthenes to aromatics and isomerization of straight to branched chain hydrocarbons of higher octane numbers (9,10). Platinum is the most important metal involved in reforming. The "platforming" process was developed by Universal Oil Products (11). However, recently EXXON has developed a new reforming catalyst containing no platinum (12). EXXON refers to its catalyst as a multimetallic cluster having three times the activity of the conventional platinum catalysts. Platinum-iridium and platinum-rhenium bimetallic impregnated Al_2O_3 catalysts are now widely used in reforming. These catalysts have a longer life (before it is necessary to regenerate them) and operate at a lower temperature with higher activity than the

old platinum catalysts. The catalyst support also plays an important role in reforming, catalyzing isomerization via a carbonium ion intermediate.

In coal liquefaction, coal is usually reacted with steam to produce CO_2, CO and H_2 with some methane present initially. The CO and H_2 undergo Fischer-Tropsch reactions to form methane and higher hydrocarbons. Hydrogenolysis catalysts can produce methane and low molecular weight hydrocarbons in one step, thus eliminating intermediate processes such as the water gas shift reaction.

Mechanistic Considerations

Hydrocarbon chemisorption involves the rupture of carbon-hydrogen bonds (13-15). At temperatures much lower than required for hydrogenolysis, the chemisorption of hydrocarbons on metals is accompanied by hydrogen evolution (16,17). The exchange reactions between paraffins and deuterium yield deutero-paraffins at temperatures lower than those needed for hydrogenolysis (18). These results indicate that carbon-hydrogen bonds are activated much more readily than carbon-carbon bonds and dehydrogenative hydrocarbon chemisorption is the initial step in hydrogenolysis (19,20). The hydrogen deficient surface species formed then undergo carbon-carbon bond scission. This is followed by reaction with hydrogen and desorption of products (21).

The surface species in ethane hydrogenolysis (14,15,22) can be 1,2 diadsorbed or adsorbed in the form of ethylidene. Hydrocarbons containing primary, secondary, tertiary, and quaternary carbons such as isobutane

and neopentane have many possible modes of adsorption. There is also evidence that the mode of hydrocarbon adsorption determines what type of reaction will occur, that is, dehydrocyclization, hydrogenolysis, or isomerization.

Anderson and Baker (23) have found the following reaction to occur for hydrocracking of hydrocarbons over nickel, tungsten, rhodium, and platinum:

1) Isomerization

2) Product formation, where the product carbon number exceeds that of the parent hydrocarbon reactant

3) Hydrogenolysis product distributions

Neopentane isomerization can occur via 1,3 diadsorption in the following manner:

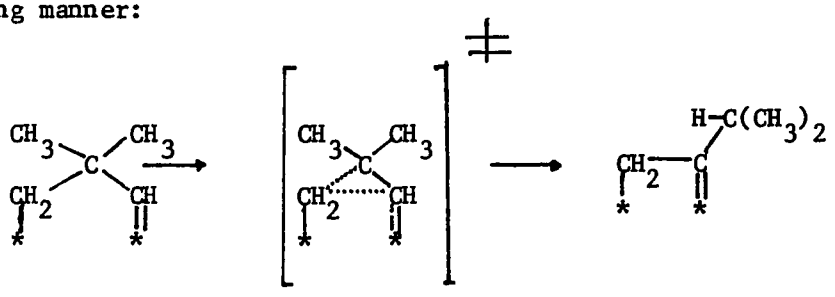

Platinum and iridum were found to be very active for this isomerization reaction by Boudart and Ptak (24). It was believed that since most work was done on supported catalysts, the support was responsible for isomerization, however Anderson and Avery (25) showed that isomerization does occur on unsupported metals and the above mechanism is most likely. Metal catalyzed isomerization is found to be energetically favorable via the previously mentioned intermediate by Hückel calculation (26). There is still some controversy over the isomerization activity of iridium. Boudart

and Ptak (24) find iridium active for isomerization reactions while Anderson and Avery (25) do not. It is believed that the more carbonium ion like the surface intermediate, the greater its isomerization probability becomes. The 1,3 diadsorbed surface species mentioned earlier is intermediate in energy between a free radical and a carbonium ion and, therefore, is very susceptible to isomerization (26). The electronegativity of the metal catalyst also plays an important role in isomerization. The more electronegative the metal, the better its chance is to obtain an electron from the surface intermediate's P_z orbital to cause double bonding to at least one carbon, favoring isomerization.

Triadsorption of isobutane on (111) platinum crystals was proposed by Anderson and Avery (25) as well as 1,3 diadsorption of isobutane to (100) platinum.

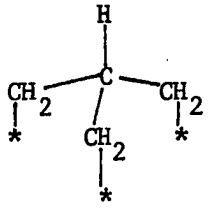

Triadsorption

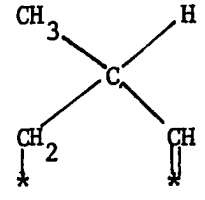

1,3 Diadsorption

The (111) face is believed to be able to accommodate the triadsorbed species better.

The apparent hydrogenolysis activation energies for the butanes and neopentane are lower than for ethane. This seems to indicate a different surface intermediate is involved. Since neopentane can not 1,2 diadsorb

but has the same activation energy as the butanes, it is believed that the butanes do not 1,2 diadsorb either.

Table 1. Hydrogenolysis on unsupported metal films[a]

Metal	Reactant	Temperature range in °C	Activation energy in kcal/mole
Pt	ethane	274-340	57
	n-butane	256-300	21
	isobutane	265-299	21
	neopentane	239-295	21
Ni	ethane	254-273	58
	propane	217-267	31
	n-butane	188-209	34
	isobutane	201-221	30
	neopentane	203-265	32
	neohexane	181-200	25

[a]From Anderson and Baker (23).

On iridium, ethane appears to 1,2 diadsorb. Neopentane either 1,3 diadsorbs or triadsorbs. On most hydrogenolysis catalysts, isobutane 1,3 diadsorbs or triadsorbs. The apparent energies of activation for hydrogenolysis on iridium are shown in Table 2. On iridium, the energy of activation for isobutane is closer to that of ethane than neopentane, therefore, 1,2 diadsorption cannot be ruled out (22,27,28). Both 1,3 diadsorption and triadsorption are conceivable models for hydrocarbon adsorption and hydrogenolysis. Energy considerations tend to favor 1,3 diadsorption for isomerization and triadsorption for hydrogenolysis. Cyclic intermediates have also been proposed for isomerization, dehydro-

Table 2. Hydrogenolysis activation energies for thin iridium films

Reference	Reactant	Temperature Range in °C	Activation energy in kcal/mole
22	ethane	100-224	25.5
27	n-heptane	135-167	25.4
28	neopentane	127-203	17.6
This thesis	isobutane	159-212	24.2

cyclization, and hydrogenolysis of cyclic and noncyclic reactants [e.g., hexane (29), cycloalkanes (30)].

Kinetics

A number of reactions can occur on the group VIII metals, of which hydrogenolysis, isomerization, and dehydrocyclization are the most important for saturated hydrocarbon reactants in the presence of hydrogen. The extent to which these reactions occur depends on the metal used and the method of catalyst preparation. Hydrogenolysis is the only reaction that occurs when ethane and hydrogen are the only reactants employed. Table 3 shows the extent to which various reactions occur on different metals.

It has been found that hydrogenolysis activity increases as dispersion increases (decreasing crystallite size) to a larger extent than could be accounted for by the corresponding increase in surface area (31,32). This increase in activity with dispersion can be attributed to electronic and geometric properties of the metal. Anderson and Avery (25) found that the (111) face of platinum isomerized isobutane to a

Table 3. Reaction of n-heptane on unsupported metals in the presence of hydrogen[a]

Metal	Pd	Rh	Ru	Pt	Ir
Temperature (°C)	300	113	88	273	125
% Hydrogenolysis	5.8	2.7	3.7	8.0	1.3
% Isomerization	0.4	0.2	0.3	10.0	0.2
% Dehydrocyclization	0.2	0.0	0.0	3.4	0.0
% Total conversion	6.4	2.9	4.0	21.4	1.5

[a] $H_2/n\text{-}C_7 = 5$, total pressure = 1 atm, rate = moles n-heptane/hr·gm from Carter, Cusumano, and Sinfelt (27).

greater extent than the (100) face, while the (100) planes had a much higher hydrogenolysis activity than the (111) surface. Hydrogenolysis activity has also been linked to the % d character of the metal bond (19,21). Thermal desorption studies show that steps and kinks are the most probable sites for hydrogenolysis (16,33,34). In the hydrogenolysis of saturated hydrocarbons possessing a number of nonequivalent carbon-carbon bonds, there is the possibility of different rates of rupture at different locations in the molecule. Of particular interest in catalysis is the product distribution associated with different metals. Nickel is highly selective for terminal carbon-carbon rupture (23,35). This is shown in Table 4. Platinum is nonselective with respect to carbon bond cleavage and all products are obtained. Some examples are given in Table 5.

Table 4. Initial products from hydrogenolysis on thick polycrystalline nickel films (mole %)[a]

Reactant	T(°C)	CH_4	C_2H_6	C_3H_8	n-C_4H_{10}	i-C_4H_{10}	n-C_5H_{12}	i-C_5H_{12}
Propane	223	88.0	12.0					
Neopentane	210	87.5	9.0	3.5				
n-Hexane	273	94.3	3.3	1.0	0.7	0.1	0.5	0.1
Methyl-cyclopropane	200	80.0	10.0					

[a]From Anderson and Baker (23), Anderson (35).

Table 5. Initial products for platinum films (mole %)[a]

Reactant	CH_4	C_2H_6	C_3H_8	n-C_4H_{10}	i-C_4H_{10}	n-C_5H_{12}	i-C_5H_{12}
Ethane	100						
n-Butane	32	29	28		11		
Isobutane	24	6	20	50			
Neopentane	14	5	4	3	10	5	59
Isobutane (111)	8	3	6	83			
Isobutane (100)	15	13	13	59			

[a]From Anderson and Avery (25); H_2/hydrocarbon = 12.

Thus far, no general rules have been developed to predict product distributions on different metals. The product distribution varies significantly depending on the catalyst employed. This is illustrated in Table 6. Product distributions also appear to depend on hydrogen pressure (36).

Table 6. The hydrogenolysis of n-heptane over unsupported metals (mole %)[a]

Metal	CH_4	C_2H_6	C_3H_8	$n\text{-}C_4H_{10}$	$n\text{-}C_5H_{12}$	$n\text{-}C_6H_{14}$
Pd	46				4	46
Rh	42	4	3	3	5	41
Ru	28	12	13	12	10	25
Pt	31	13	17	16	9	14
Ir	21	21	15	14	14	15

[a]Carter, Cusumano and Sinfelt (27); P_{total} = 1 atm, $H_2/n\text{-}C_7$ = 5.

There are very few papers in the literature dealing with the hydrogenolysis of isobutane on iridium (25,36). Most kinetic studies were done on ethane in very narrow pressure ranges. Typically, the kinetic data were fit to a power rate law of the form:

$$R = k(P_{hydrocarbon})^M (P_{H_2})^N.$$

For ethane hydrogenolysis the hydrogen order was usually negative while the ethane reaction order was usually reported as positive. This type of analysis was also applied to larger hydrocarbons such as propane, the butanes and the pentanes. Table 7 shows some reaction orders for

Table 7. Isobutane hydrogenolysis orders

Reference	Catalyst	Temperature range °C	Isobutane order	Hydrogen order	Pressure range
25	Pt film	265-299	+.5	+1.4	P_{H_2} = 11-44 torr
					P_{ISO} = .9-3.4 torr
25	Pd film	270-311	-.2	+ .1	same as above
36	Ru/Al_2O_3	85-130	+.74	- .66	P_{H_2} = 400-700 torr
					P_{ISO} = 66-400 torr

isobutane obtained in this way. The ruthenium study (36) was done in a stirred tank reactor.

Later studies showed reaction orders to be a function of reactant partial pressures. The following sequence of reactions was first proposed by Cimino, Boudart and Taylor (3) as the mechanism of ethane hydrogenolysis on iron:

$$2* + C_2H_6(9) \underset{k-1}{\overset{k_1}{\rightleftharpoons}} C_2H_5* + H*$$

$$C_2H_5* + H* \overset{K_2}{\rightleftharpoons} C_2H_x** + aH_2(g)$$

$$C_2H_x** + H_2(g) \overset{K_3}{\rightleftharpoons} CH_x* + CH_z*$$

$$(4-z)H_2(g) + CH_z* \overset{K_4}{\rightleftharpoons} CH_4(g) + * \qquad a = \frac{6-x}{2}$$

Step 3 is postulated to be the rate limiting step. Using a steady state treatment, assuming that step 2 is at equilibrium leads to the following relations.

$$K_2 = \frac{\theta_{C_2H_x} P_{H_2}^{a}}{\theta_{C_2H_5} \theta_H}$$

$$k_1 P_{C_2H_6} - k_{-1} \theta_{C_2H_5} \theta_H = k_3 \theta_{C_2H_x}$$

The rate of the reaction is the rate of the slowest step:

$$r = k_3 \theta_{C_2H_x} P_{H_2}$$

$$\theta_{C_2H_x} = \frac{k_1 P_{C_2H_6}}{[k_3 P_{H_2} + \frac{k_{-1}}{k_2} P_{H_2}^{a}]}$$

$$r = \frac{k_1 P_{C_2H_6}}{[1 + \frac{k_{-1}}{k_2 k_3} P_{H_2}^{a-1}]}$$

The above mechanism assumes reversible hydrocarbon adsorption. Carbon bond scission is postulated as the rate limiting process. This mechanism has also been applied to higher hydrocarbons. The general scheme for the hydrogenolysis of higher hydrocarbons is:

$$C_N H_{2N+2} \rightleftharpoons C_N H_{2N+2-2a}(ads) + aH_2$$

$$C_N H_{2N+2-2a}(ads) + H_2 \longrightarrow C_x H_y(ads) + C_{N-x} H_z(ads)$$

$$C_x H_y(ads) \longrightarrow \text{Products}$$

$$C_{N-x} H_z(ads) \longrightarrow \text{Products}$$

Most kinetic data for higher hydrocarbon hydrogenolysis is fit by an expression of the form:

$$R = \frac{A\, P_{HC}}{[1 + B\, P_{H_2}^{a-1}]}$$

The problem with Boudart's mechanism is that it could not account for positive hydrogen orders or negative hydrocarbon reaction orders. It also assumed that hydrocarbon adsorption was reversible. In both respects, it is not satisfactory for treating hydrogenolysis on iridium. The elementary reactions used by Boudart assume hydrogen is liberated during hydrocarbon chemisorption and the carbonaceous surface layer is hydrogenated by gas phase hydrogen. However, alternate mechanisms can be used to explain hydrogenolysis based on surface hydrogen being used to hydrogenate surface carbon to form methane as well as other hydrocarbons.

Table 8 shows some product distributions for isobutane on various metal catalysts.

Table 8. Isobutane product distributions (mole %)[a]

Catalyst	CH_4	C_2H_6	C_3H_8	$n\text{-}C_4H_{10}$	Reference
W film	59	6	33	2	23
Pt film	15	8	19	58	23
Ni film	70	5	10	15	23
Pd film	49	1	47	3	25
Ru/Al_2O_3	58	29	13	0	35

[a] H_2/hydrocarbon > 1 (23), 5 (25); P_{total} = 800, H_2/hydrocarbon = 30 → 1 (36).

Research Objectives

The purpose of this research project is to establish the mechanism of hydrogenolysis of isobutane on iridium. Kinetic data were obtained over a range of pressure spanning three orders of magnitude (.1 - 100 torr). The kinetic data obtained displayed the entire variation of kinetic orders with respect to the partial pressure of both reactants. The activation energy for hydrogenolysis was also determined. A detailed mechanism is provided and derived rate expressions have been fit to the experimental data.

EXPERIMENTAL

Experimental Techniques

A pyrex glass and 304 stainless steel system pumped by rotor pumps, mercury diffusion pumps and an ion pump was used to collect kinetic data. A schematic of the system is shown in Figure 1. The system is divided into a low vacuum and a high vacuum side; the high vacuum side consists of the mass spectrometer, ion pump and reaction cell. The low vacuum side consists of the manifold and capacitance manometer. Gases were premixed in the manifold before being exposed to the catalyst during kinetic experiments. Pressures were measured by the capacitance manometer (MKS Series 315 Head) in the .1 - 100 torr range and by conventional Bayard-Albert ionization gauge in the 1×10^{-10} - 1×10^{-4} torr range. The capacitance manometer was calibrated against a McLeod gauge (Consolidated Vacuum Corporation, Type GM100A, Rochester, New York) using argon. Calibration curves were linear having the form:

$$\text{Pressure (torr)} = C\ (\text{scale reading}) + D$$

To prevent zero drift, the manometer head was thermostated at 50°C.

The best manifold vacuum was 1×10^{-7} torr. This was obtained by a double stage diffusion pump in series with an LN_2 trap. The high vacuum side could be pumped to 1×10^{-9} torr with a 20 l/s differential ion pump (Ultek, Model #60-063), after attaining a vacuum of 1×10^{-8} torr via double and triple stage diffusion pumps in series with an $L\text{-}N_2$ trap.

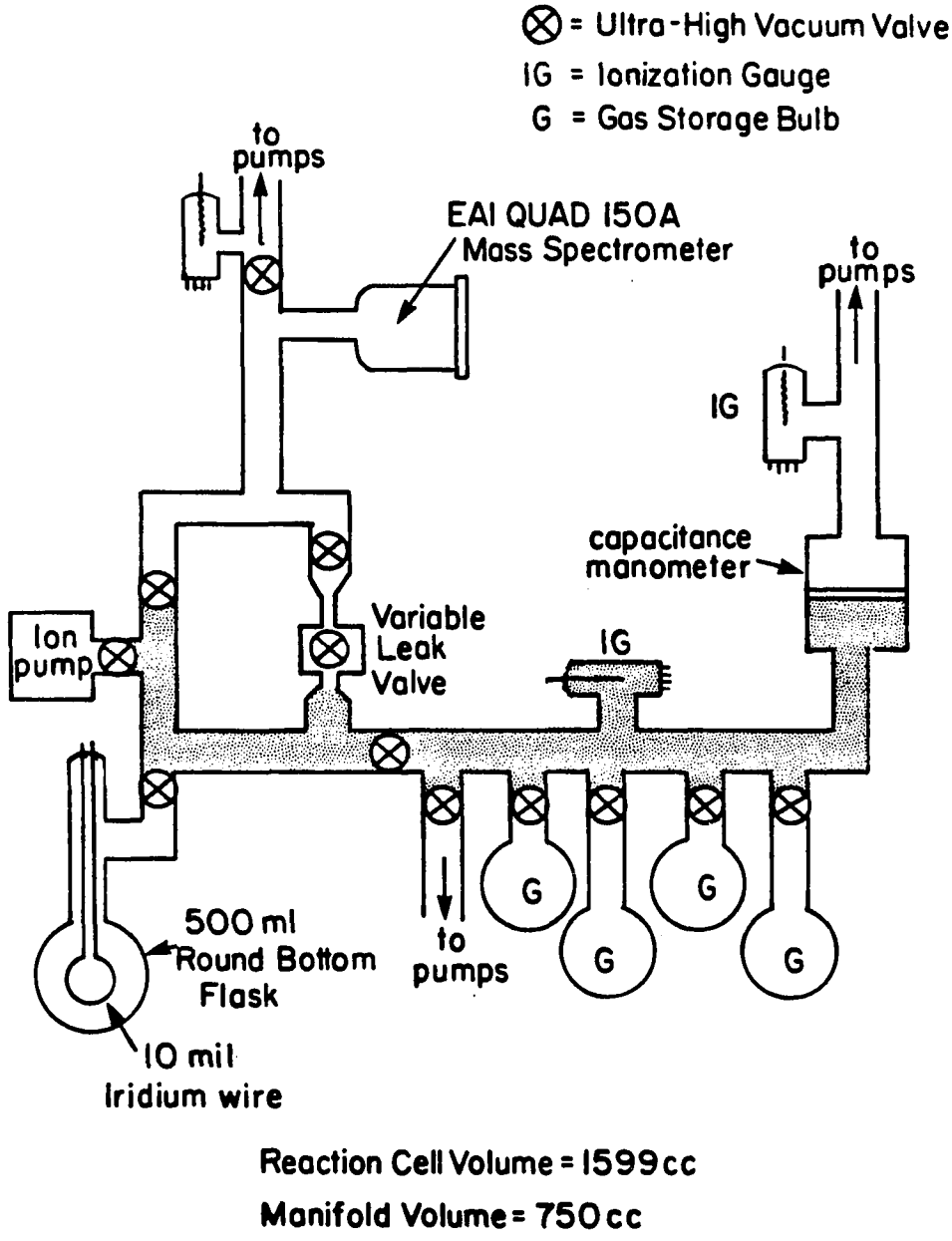

Figure 1. Experimental techniques-high vacuum system

The high vacuum side includes a 500 ml round bottom flask reaction cell in which an iridium wire (10 cm long, 10 mil thick) was spot welded to two tungsten support posts. The reaction cell was heated by a tube furnace (S. B. Lindberg, Watertown, Wisconsin) between room temperature and 250°C. The temperature was monitored by a chromel-alumel thermocouple in direct contact with the reaction cell glass. At equilibrium, the temperature remained constant to within ±1.5°C.

The reactor system was static; reaction mixtures were leaked from the reaction volume (reaction cell plus manifold) through a leak valve (Granville-Phillips Company, Series 203, Boulder, Colorado) to the differentially pumped mass spectrometer (AEI Quad 150A).

The leak valve was variable and was set so only 1.7% of the reactants were leaked out of the reaction volume during a kinetic run usually lasting two minutes. The mass spectrometer signal was monitored by a dual channel horizontal readout rectilinear thermal writing oscillographic recorder (Soltec Corporation, 8K21 Series, Sun Valley, California). Various mass to charge peaks were monitored depending on the experiment performed. Typically the M/e = 16 peak was observed every 1 second for two minutes during a kinetic run. Peak finding was facilitated by an oscilloscope (Tektronix Inc., Type RM503).

The volumes of the manifold and reaction cell were needed in order to determine the number of molecules of reactants and products present. This was easily done by attaching a standard volume to the manifold and using the relationship $P_1V_1 = P_2V_2$. The reaction cell volume was found to be

1599 cc and the manifold volume was 750 cc. The system was baked out to 350°C using a portable oven and heating tapes prior to a series of kinetic experiments. The capacitance manometer head had to be baked out periodically because of fluctuations due to adsorbed gases.

The mass spectrometer consisted of three main sections: the ionization region, the quadrupole region and the electron multiplier. In the ionization chamber, gas molecules are ionized by 80-volt electrons emitted by a tungsten 3% rhenium filament heated by a variable current of .25 to 3.0 milliamps. The emitted ions are then accelerated and focused by electrostatic lenses into the quadrupole filter where they are separated on the basis of their M/z ratios. The ions are then swept through a filter in order of increasing M/z values. The intensity of the output signal (voltage) from the electron multiplier is directly proportional to the pressure of the gas entering the mass spectrometer. Rates were measured in terms of voltage change per unit time and converted into molecules per second via mass spectrometer calibration curves and the ideal gas law. For the pressure range employed in the kinetic experiments, the mass spectrometer calibration curves were linear (the mass spectrometer was calibrated against the capacitance manometer). The mass spectrometer was calibrated periodically and was found to vary ±6%. It was also found that the mass spectrometer signal varied negligibly with the incoming gas temperature (.1% per degree centigrade).

Materials

The gases used in all experiments were contained in glass bulbs equipped with break seals. In general, gases were of ultrahigh purity. Methane (99.99%), argon (99.9995%) and hydrogen (99.9995%) were obtained from Union Carbide, Linde Division (Chicago, Illinois) in one liter glass bulbs. A lecture bottle of isobutane (99.96%) was obtained from Matheson Gas Products (Joliet, Illinois) and was loaded into a glass bulb in a high vacuum system after being purified by repeated distillations using $L\text{-}N_2$. Deuterium (99.99%) was purchased from Air Products and Chemicals Inc. (Los Angeles, California) in a glass bulb. Ten mil iridium wire was obtained from Engelhard Industries (Newark, N.J.).

Thin Film Deposition

Prior to deposition of the catalyst, calibration curves were obtained for the mass spectrometer and the system was baked out at approximately 250°C for 12 hours. All ion gauges were degassed and the reaction cell was baked out again with a tube furnace. During this second bakeout the tungsten support posts and the iridium wire spot welded to them were degassed by resistive heating with a constant current power supply ($T_{\text{iridium wire}} = 1339°C$).

The high vacuum side was employed in film deposition since it attained the lowest ambient pressure (1×10^{-9} torr). The current was increased gradually while the iridium wire temperature was monitored by an optical pyrometer. The system pressure was checked by an ion gauge. When

the current was increased the pressure gradually increased, reached a maximum then decreased. It was found that films deposited in an ambient pressure greater than 5×10^{-8} torr were catalytically inactive. Therefore, the current was always regulated to keep the pressure lower than 5×10^{-8} torr. The reaction cell was at room temperature during film deposition (previous studies show this gave the most active films). The weight of the catalyst deposited can be calculated in two ways. The first involves using the following equation:

$$\log W = 9.98 - .51 \log T(K) - \frac{3100}{T(K)}$$

From Dushman (37)

where W = rate of metal evaporation in g/cm^2 sec from a wire of surface area .80 cm^2

T = temperature in K.

Using the geometric surface area of the glass bulb (303.62 cm^2) and the bulk density of iridium (22.45 g/cc), the film thickness can be calculated. The following table shows the weight and thickness of the film used. The second method consists of weighing the wire before and after deposition; this gave 3.0 mg. After catalyst deposition, the film was sintered for 1 hour at 250°C in 1 torr of hydrogen. An active film was maintained by storing the film in hydrogen when it was not in use (1 torr). In general, films were cleaned by heating them 20°C higher than the reaction temperature in 1 torr of hydrogen until all carbon was removed from the catalyst's surface as determined by the mass spectrometer. Cleaning was considered complete when the methane signal remained constant.

Table 9. Thin film deposition data[a,b]

Current (ma)	Iridium wire temperature, K	Time (sec)	Deposition rate g/s	Weight deposited, g
3.4	1813	1020	8.98×10^{-10}	9.17×10^{-7}
3.8	1858	2640	4.39×10^{-9}	11.59×10^{-6}
4.0	1893	1920	4.71×10^{-9}	9.04×10^{-6}
4.2	1935	720	1.03×10^{-8}	7.42×10^{-6}
4.4	1972	2520	2.10×10^{-8}	5.29×10^{-6}
4.6	2008	1200	4.01×10^{-8}	4.81×10^{-6}
4.8	2047	240	7.82×10^{-8}	1.88×10^{-6}
5.0	2100	1980	1.92×10^{-7}	3.80×10^{-6}
5.1	2104	720	2.06×10^{-7}	1.48×10^{-6}
5.2	2123	300	2.71×10^{-7}	8.13×10^{-5}
5.4	2161	1620	4.93×10^{-7}	7.99×10^{-4}
5.6	2199	2220	8.77×10^{-7}	1.95×10^{-3}

[a]Total weight deposited 3.30 mg.

[b]Film thickness 48.5 Å.

RESULTS AND DISCUSSION

Kinetics and Adsorption

The two main models employed in heterogeneous catalysis are the Langmuir Hinshelwood and Rideal Eley mechanisms. In the first scheme, two or more chemisorbed species react to give gaseous product upon desorption. The second mechanism involves a reaction between a chemisorbed species and either a gas phase or physisorbed reactant to give product. Both models are derived for the simplest cases below. In both models, adsorption is the first step.

$$A(g) + * \underset{}{\overset{K_A}{\rightleftharpoons}} A*$$

$$B(g) + * \underset{}{\overset{K_B}{\rightleftharpoons}} B*$$

$$K_A = \frac{(A*)}{P_A(*)} \qquad K_B = \frac{(B*)}{P_B(*)}$$

Surface site conservation gives an expression for the free surface site concentration (*).

$$1 = (A*) + (B*) + (*)$$

$$(*) = \frac{1}{[1 + K_A P_A + K_B P_B]}$$

The Langmuir Hinshelwood rate limiting step gives rise to the following expression.

$$A^* + B^* \xrightarrow{k} \text{Products}$$

$$\frac{d[\text{Products}]}{dt} = k(A^*)(B^*) = kK_AK_B\ P_AP_B(^*)^2 = \frac{kK_AK_B\ P_AP_B}{[1 + K_AP_A + K_BP_B]}\ ^2$$

The Rideal Eley approach leads to the rate equation depicted below.

$$A^* + C(g) \xrightarrow{k} \text{Products}$$

$$\frac{d[\text{Products}]}{dt} = kP_C(A^*) = kK_AP_AP_C(^*) = \frac{kK_A\ P_AP_C}{[1 + K_AP_A + K_BP_B]}$$

Order plots (that is plots of log rate vs log partial pressure) can be used to distinguish between the two different mechanisms.

In order to be able to compare rates obtained from different catalysts, product production is usually reported as a rate per unit weight of catalyst or per catalyic site. Throughout this thesis, rates will be reported in the form of turnover numbers (molecules/site • sec).

For the hydrogenolysis of isobutane on iridium, the sole reaction product is methane; no other hydrocarbons are observed experimentally. For every isobutane molecule consumed, four methane molecules are produced. The mechanism employed to explain the experimental data in this thesis assumes that the surface is only covered with monocarbon fragments, that is, isobutane degradation is fast and complete. If the assumption is made that each methane comes from a monocarbon fragment occupying one active site then the number of monocarbon fragments on the surface equals the

number of active sites occupied. Therefore, methane desorption can be used to determine the number of active sites.

Figure 2 shows methane desorption as a function of isobutane partial pressure under reaction conditions. The hydrogen pressure is held constant. The following procedure was employed in obtaining these data. A premixed ratio of reactant gases was exposed to the catalyst at reaction temperature. After the reaction rate was measured, the reaction gases were pumped away. The catalyst was then cleaned by heating in hydrogen. The methane desorbing from the surface was monitored by the mass spectrometer. When the methane signal remained constant with respect to time, cleaning was considered complete. The number of methane molecules can be calculated by taking into account the reaction cell volume and temperature, the manifold volume and temperature and the ideal gas law. Extrapolation to the limiting value at high isobutane pressure gives the maximum number of monocarbon fragments on the surface at the reaction temperature, which is equal to the number of active sites.

An alternate method of determining the number of active sites can be used as a check; this method is depicted in Figure 3. Again, a premixed ratio of reactant gas is exposed to the catalyst and the reaction rate is measured. The reaction cell is pumped down and the catalyst is cleaned by heating in hydrogen. In this experiment, the hydrogen pressure is varied while the isobutane pressure is held constant. Extrapolation gives the methane coverage at zero hydrogen present. Both of these methods take advantage of the competition between hydrogen and isobutane car-

Figure 2. Methane desorption as a function of isobutane pressure at 209°C

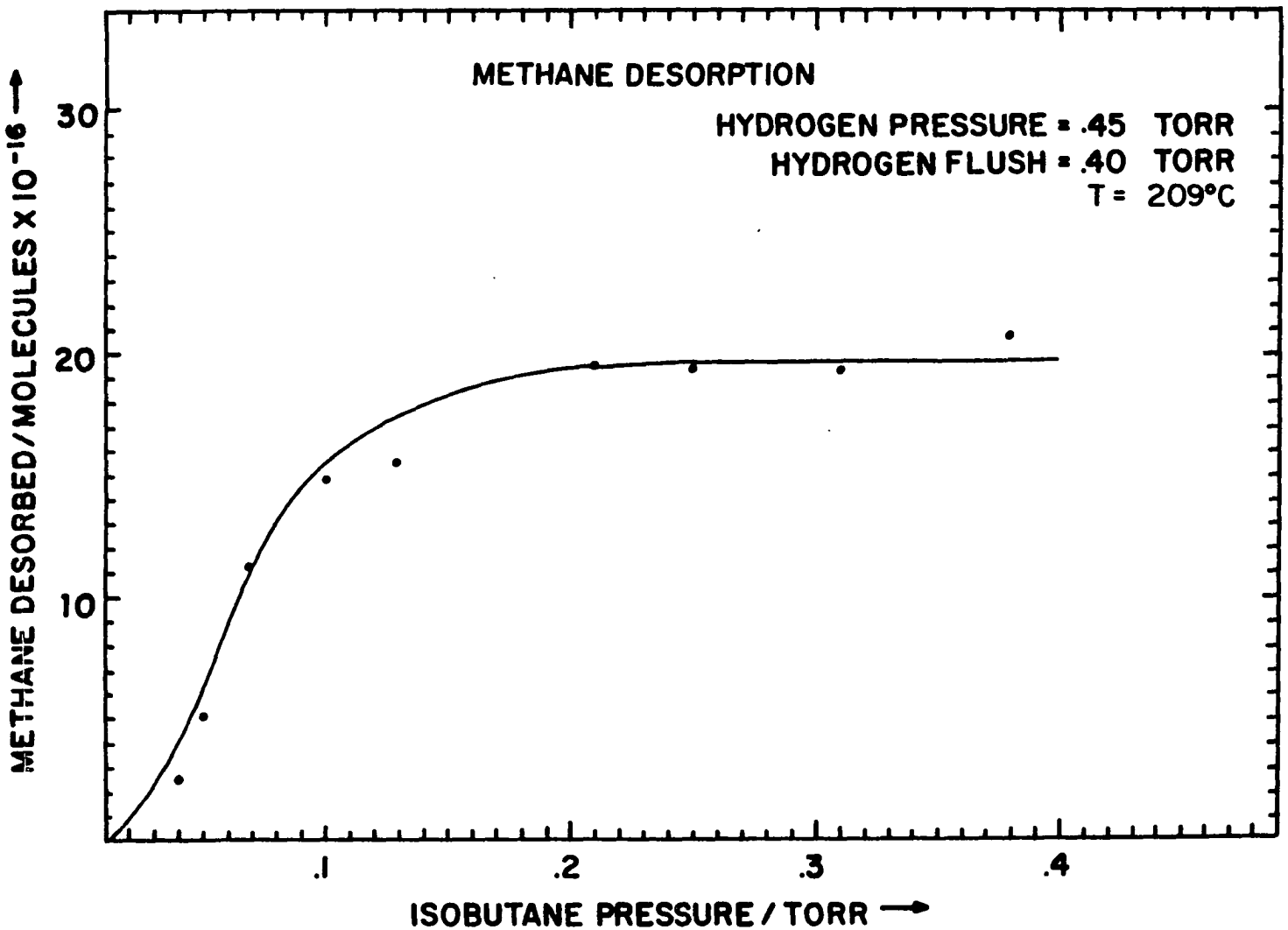
METHANE DESORPTION
HYDROGEN PRESSURE = .45 TORR
HYDROGEN FLUSH = .40 TORR
T = 209°C
METHANE DESORBED/MOLECULES X 10⁻¹⁶ →
30
20
10
.1
.2
.3
.4
ISOBUTANE PRESSURE / TORR →

Figure 3. Methane desorption as a function of hydrogen pressure at 209°C

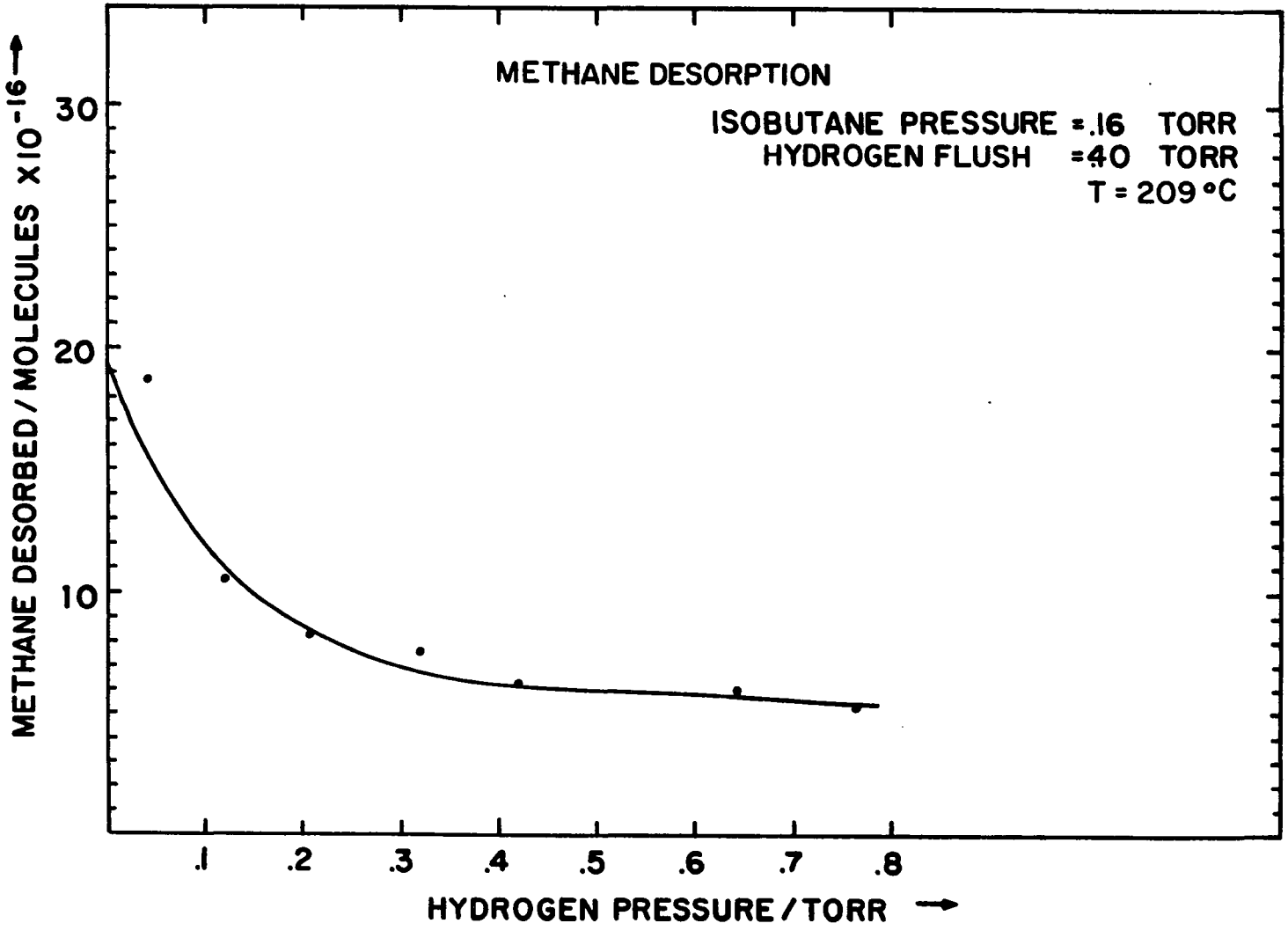
METHANE DESORPTION
ISOBUTANE PRESSURE =.16 TORR
HYDROGEN FLUSH =40 TORR
T = 209 °C
METHANE DESORBED / MOLECULES X10⁻¹⁶
30
20
10
.1
.2
.3
.4
.5
.6
.7
.8
HYDROGEN PRESSURE / TORR

bon fragments for surface sites on iridium. Both figures are essentially Langmuir adsorption isotherms involving competitive adsorption. The average number of surface sites available on iridium at 209°C is shown below.

$$N_{MAX}(209°C) = 20 \times 10^{16} \text{ sites}$$

The number of active sites calculated here implies nothing about the number of metal atoms involved in the catalytic process. For example, methane may be bound to the surface in the following forms:

$$CH_3^* \qquad CH_2^* \qquad CH^* \qquad \text{or} \qquad C^*,$$

where * refers to a bond between carbon and an active site. Bonding to an active site may involve single, double or triple carbon to metal bonds. Carbon may even be bound to two or more metal atoms simultaneously. Some possible surface bondings are depicted below.

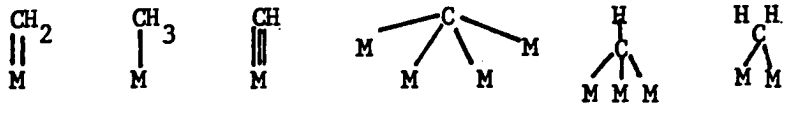

As stated earlier, the only reaction product observed was methane. It was also observed experimentally that for every isobutane consumed four methane molecules were produced; therefore, the net chemical reaction for the hydrogenolysis of isobutane on iridium is:

$$C_4H_{10}(g) + 3H_2(g) = 4CH_4(g)$$

Deuterium exchange with isobutane on iridium was not observed at 175°C to 209°C; however, earlier investigations have shown that exchange reactions become significant at lower temperatures on iridium (22). It appears that above 170°C hydrogenolysis is the primary reaction. Hydrocarbon adsorption is irreversible and carbon-carbon bond scission is complete, yielding only monocarbon surface fragments. When isobutane was exposed to the catalyst at 175°C and 209°C for 10 minutes, the gas ambient pumped away and deuterium admitted to the reaction cell the largest peak observed via the mass spectrometer was due to CH_2D_2. No other peaks were observable in the 16 a.m.u. to 20 a.m.u. mass range. It appears that CH_2* is the major surface species remaining after pump down; while some C* and CH* may exist, these surface concentrations must be very small or CHD_3 and CD_4 would have been observed on deuteration.

Thermal desorption studies also showed isobutane to be irreversibly adsorbed while hydrogen and methane are reversibly adsorbed to iridium. Methane is reversibly adsorbed in that after adsorption hydrogenation can recover the adsorbed carbon in the form of CH_4. In the present work, however, methane partial pressures were always sufficiently small so that the contribution of gaseous methane to surface monocarbon fragments was negigible.

Thermal desorption spectra show two overlapping peaks for hydrogen on polycrystalline iridium. The low temperature peak at 110°C is characteristic of low index crystal faces while the peak appearing at 160°C is due to the interaction of hydrogen with stepped and high index crystal

planes. This was also observed by Somorjai and Weinberg (33,34,38,39). Hydrogen adsorption on iridium is very similar to hydrogen adsorption on platinum (40,41). Since hydrogen is bound more strongly to the kinks, it is possible that hydrocarbon decomposition occurs to a greater extent on the kinks than on low index planes. Observation of the thermal desorption spectra of hydrogen arising from carbon fragments on the surface after exposing the catalyst to isobutane showed three peaks. Two hydrogen peaks were due to atomically adsorbed hydrogen (110°C and 160°C). The third peak was centered at 320°C and was due to hydrogen associated with carbonaceous fragments on the surface. This has also been observed for a number of hydrocarbons on iridium in the literature (16,38,39). The thermal desorption spectra are shown in Figures 4 and 5. Thermal desorption spectra were obtained in the following manner. Isobutane or hydrogen was admitted to the reaction cell at room temperature. Each exposure was for 10 minutes until an equilibrium presence was observed. The ambient gas was then pumped away and heating was accomplished by a tube furnace with a powerstat. The heating rate was 8.4°C/min.

Since deuterium exchange with isobutane on iridium is not appreciable above 170°C and only monocarbon fragments are recovered from the catalyst's surface (mostly CH_2*), it appears that isobutane as well as its decomposition products are irreversibly adsorbed in the 175-209°C temperature regime. The following sequence of reactions can account for this if the reverse steps are considered negligible.

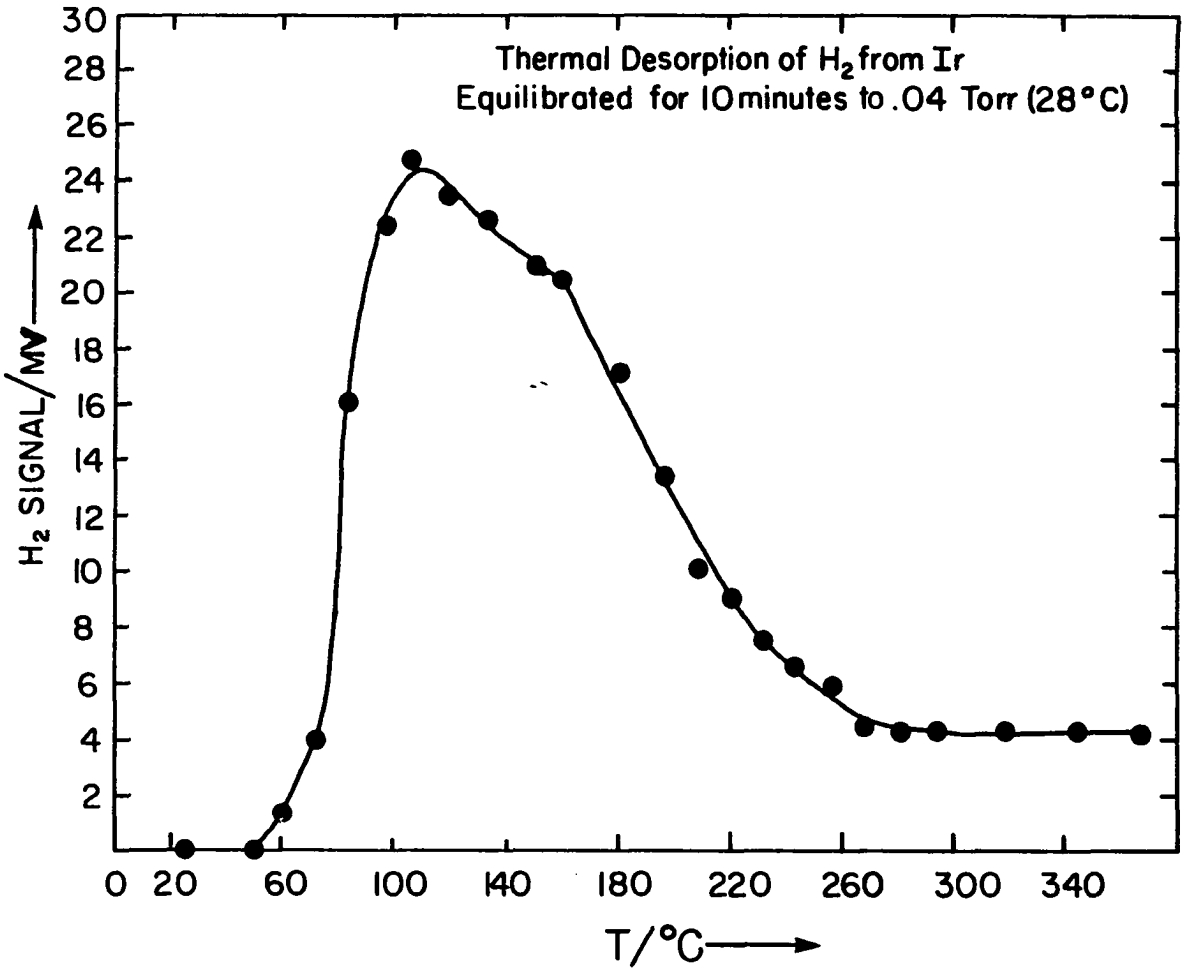

Figure 4. Thermal desorption spectrum of H_2 on Ir

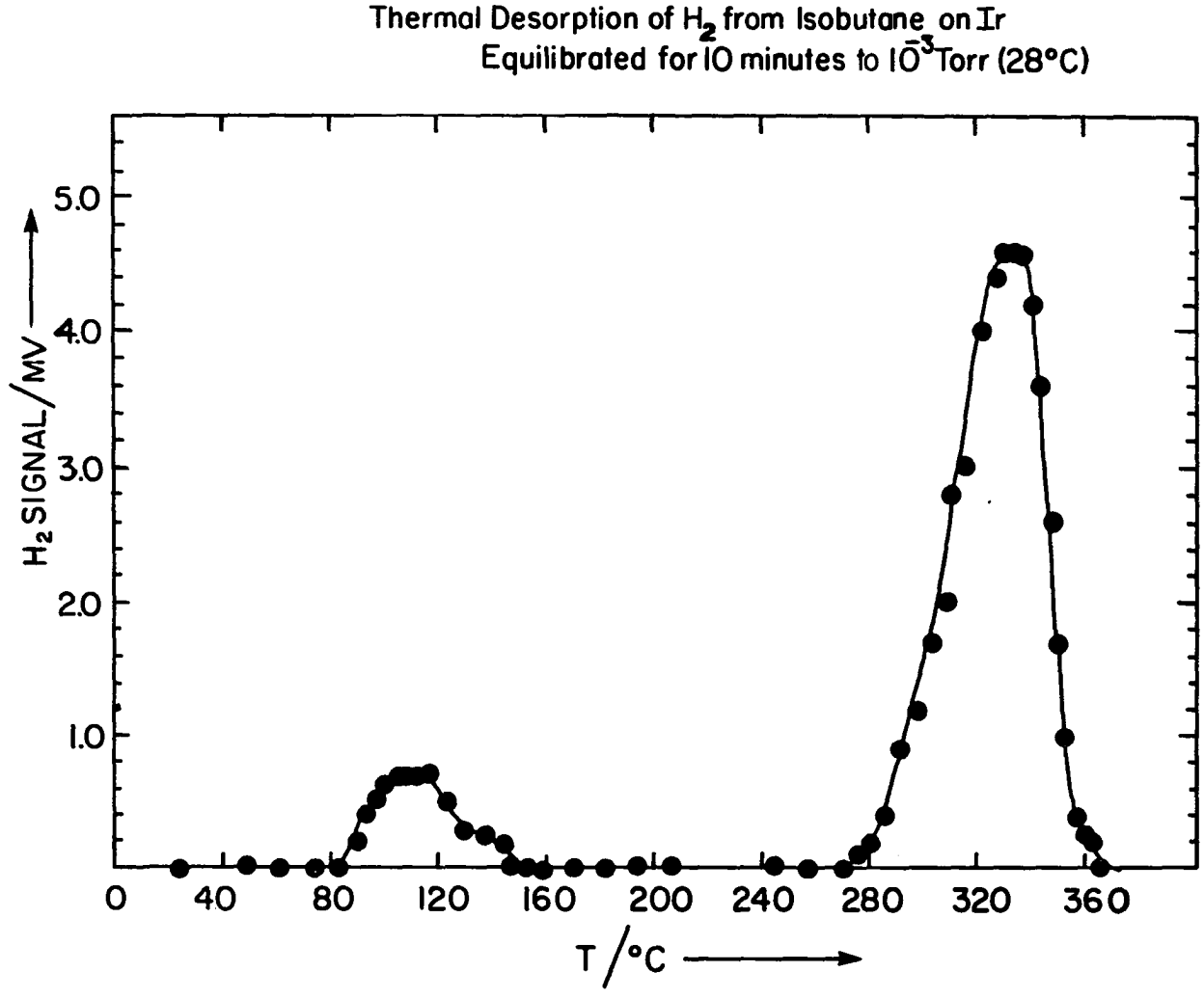

Figure 5. Thermal desorption spectrum of hydrogen from hydrocarbon fragments on Ir

$$C_4H_{10}(g) + 2* \underset{k-1}{\overset{k_1}{\rightleftharpoons}} C_4H_9* + H*$$

$$C_4H_9* + * \underset{k-2}{\overset{k_2}{\rightleftharpoons}} C_4H_8* + H*$$

$$C_4H_8* + * \underset{k-3}{\overset{k_3}{\rightleftharpoons}} C_3H_6* + CH_2*$$

$$C_3H_6* + * \underset{k-4}{\overset{k_4}{\rightleftharpoons}} C_3H_5* + H*$$

$$C_3H_5* + * \underset{k-5}{\overset{k_5}{\rightleftharpoons}} C_2H_3* + CH_2*$$

$$C_2H_3* + * \underset{k-6}{\overset{k_6}{\rightleftharpoons}} C_2H_2* + H*$$

$$C_2H_2* + * \underset{k-7}{\overset{k_7}{\rightleftharpoons}} C* + CH_2*$$

The reverse reactions are included here because as temperature is decreased the reverse steps will become more significant. This will account for deuterium exchange results involving surface species maintaining their gas phase carbon skeletal features. The adsorption of hydrogen to the catalyst has been shown to occur via thermal desorption studies. Surface hydrogen and monocarbon fragments react in a Langmuir Hinshelwood fashion to give methane, as depicted below.

$$C* + H* \underset{k-8}{\overset{k_8}{\rightleftharpoons}} CH* + *$$

$$CH^* + H^* \underset{k_{-9}}{\overset{k_9}{\rightleftharpoons}} CH_2^* + *$$

$$CH_2^* + H^* \underset{k_{-10}}{\overset{k_{10}}{\rightleftharpoons}} CH_3^* + *$$

$$CH_3^* + H^* \underset{k_{-11}}{\overset{k_{11}}{\rightleftharpoons}} CH_4(g) + 2*$$

$$H_2(g) + 2* \underset{k_{-12}}{\overset{k_{12}}{\rightleftharpoons}} 2H^*$$

Multiplying reactions 10 and 11 by a factor of four, taking reaction 12 three times and summing gives the net reaction:

$$C_4H_{10}(g) + 3H_2(g) = 4CH_4(g)$$

The steady state hypothesis can be employed to give a set of simultaneous equations which can be solved for surface intermediate concentrations.

For the nonmonocarbon surface species:

$$\frac{d(\text{surface intermediate})}{dt} = 0$$

$$k_1 P_{C_4H_{10}} (*)^2 = k_2(C_4H_9*)(*) = k_3(C_4H_8*)(*)$$

$$= k_4(C_3H_6*)(*) = k_5(C_3H_5*)(*)$$

$$= k_6(C_2H_3*)(*) = k_7(C_2H_2*)(*)$$

The above equalities hold because the reverse steps of reactions one through seven are considered negligible.

The surface concentration of nonmonocarbon fragments is given by the following summation.

$$\sum_{N=2}^{4} (C_N H_X *) = \sum_{i=2}^{7} \frac{k_1}{k_i} P_{C_4H_{10}}(*)$$

For monocarbon surface species, the steady state relations give rise to the following equations.

$$\frac{d(C*)}{dt} = 0;\ k_8(C*)(H*) - k_{-8}(CH*)(*) = k_7(C_2H_2*)(*)$$

$$= k_1 P_{C_4H_{10}}(*)^2$$

$$\frac{d(CH*)}{dt} = 0;\ k_9(CH*)(H*) - k_{-9}(CH_2*)(*) = k_8(C*)(H*) - k_{-8}(CH*)(*)$$

$$\frac{d(CH_2*)}{dt} = 0;\ k_{10}(CH_2*)(H*) - k_{-10}(CH_3*)(*) = 4k_1 P_{C_4H_{10}}(*)^2$$

The stoichiometry of the reaction requires the rate of methane production to be four times the rate of isobutane consumption.

$$\frac{d(CH_3*)}{dt} = 0;\ k_{11}(CH_3*)(H*) - k_{-11} P_{CH_4}(*)^2 = 4k_1 P_{C_4H_{10}}(*)^2$$

The reverse of reaction eleven is negligible for the pressure of methane observed, therefore:

$$k_{11}(CH_3*)(H*) = 4k_1 P_{C_4H_{10}}(*)^2.$$

For the surface hydrogen:

$$\frac{d(H^*)}{dt} = 0;\ k_{12} P_{H_2} (*)^2 - 3k_1 P_{C_4H_{10}} (*)^2 = k_{-12}(H^*)^2$$

When $k_1 << k_{12}$ (experimentally verified later) hydrogen adsorption can be considered to be at equilibrium.

$$(H^*) = K_{12}^{\frac{1}{2}} P_{H_2}^{\frac{1}{2}} (*)$$

The monocarbon surface fragment concentrations are shown below.

$$(CH_3^*) = \frac{4k_1}{k_{11}} \frac{P_{C_4H_{10}} (*)^2}{(H^*)}$$

$$(CH_2^*) = \frac{4k_1 P_{C_4H_{10}} (*)^2}{k_{10} (H^*)} + \frac{4k_{-10} k_1 P_{C_4H_{10}} (*)^3}{k_{10} k_{11} (H^*)^2}$$

$$(CH^*) = \frac{4k_1 P_{C_4H_{10}} (*)^2}{k_9 (H^*)} + \frac{4k_{-9} k_1 P_{C_4H_{10}} (*)^3}{k_9 k_{10} (H^*)^2} + \frac{4k_{-9} k_{-10} k_1 P_{C_4H_{10}} (*)^4}{k_9 k_{10} k_{11} (H^*)^3}$$

$$(C^*) = \frac{4k_1 P_{C_4H_{10}} (*)}{k_8 (H^*)} + \frac{4k_{-8} k_1}{k_8 k_9} \frac{P_{C_4H_{10}} (*)^3}{(H^*)^2}$$

$$+ \frac{4k_{-8}}{k_8} \frac{k_{-9}}{k_9} \frac{k_1}{k_{10}} \frac{P_{C_4H_{10}} (*)^4}{(H^*)^3} + \frac{4k_{-8}}{k_8} \frac{k_{-9}}{k_9} \frac{k_{-10}}{k_{10}} \frac{k_1}{k_{11}} \frac{P_{C_4H_{10}} (*)^5}{(H^*)^4}$$

The conservation of surface site expression is:

$$1 = (*) + (C_4H_9*) + (C_4H_8*) + (C_3H_6*) + (C_3H_5*)$$

$$+ (C_2H_3*) + (C_2H_2*) + (CH_3*) + (CH_2*)$$

$$+ (CH*) + (C*) + (H*)$$

Assuming that the monocarbon fragments predominate on the surface, as the experimental results suggest, the following simplified surface site conservation expression is obtained.

$$1 = (*) + (H*) + (CH*) + (CH_2*) + (CH*) + (C*)$$

$$(*) = [1 + \sqrt{K_{12}}\, P_{H_2}^{\frac{1}{2}} + \frac{4k_1\, P_{C_4H_{10}}}{\sqrt{K_{12}}\, P_{H_2}^{\frac{1}{2}}} (\frac{1}{k_8} + \frac{1}{k_9} + \frac{1}{k_{10}} + \frac{1}{k_{11}})$$

$$+ \frac{4k_1\, P_{C_4H_{10}}}{K_{12}\, P_{H_2}} (\frac{1}{k_{11}\, K_{10}} + \frac{1}{k_{10}\, K_9} + \frac{1}{k_9\, K_8})$$

$$+ \frac{4k_1\, P_{C_4H_{10}}}{K_{12}^{3/2}\, P_{H_2}^{3/2}} (\frac{1}{k_{11}\, K_{10}\, K_9} + \frac{1}{k_{10}\, K_9\, K_8})$$

$$+ \frac{4k_1\, P_{C_4H_{10}}}{K_{12}^{2}\, P_{H_2}^{2}} (\frac{1}{k_{11}\, K_{10}\, K_9\, K_8})]^{-1}$$

The rate expression is defined in terms of hydrocarbon adsorption.

$$C_4H_{10}(g) + 2* \xrightarrow{k_1} C_4H_9* + H*$$

$$R = -4\frac{d(P_{C_4H_{10}})}{dt} = \frac{dP_{CH_4}}{dt} = 4k_1 P_{C_4H_{10}} (*)^2$$

$$R = A P_{C_4H_{10}} / [1 + B P_{H_2}^{\frac{1}{2}} + \frac{C P_{C_4H_{10}}}{P_{H_2}^{\frac{1}{2}}} + \frac{D P_{C_4H_{10}}}{P_{H_2}}$$

$$+ \frac{E P_{C_4H_{10}}}{P_{H_2}^{3/2}} + \frac{F P_{C_4H_{10}}}{P_{H_2}^{2}}]^2$$

The above rate equation can be expressed in a linear form at fixed hydrogen pressure in the following way.

$$\sqrt{\frac{P_{C_4H_{10}}}{R}} = \frac{1}{A^{\frac{1}{2}}} \left[\frac{C}{P_{H_2}^{\frac{1}{2}}} + \frac{D}{P_{H_2}} + \frac{E}{P_{H_2}^{3/2}} + \frac{F}{P_{H_2}^{2}} \right] P_{C_4H_{10}} + \frac{1 + B P_{H_2}^{\frac{1}{2}}}{A^{\frac{1}{2}}}$$

where $A = 4k_1$

$B = K_{12}$

$$C = \frac{4k_1}{\sqrt{K_{12}}} \left(\frac{1}{k_8} + \frac{1}{k_9} + \frac{1}{k_{10}} + \frac{1}{k_{11}}\right)$$

$$D = 4k_1/K_{12} \left(\frac{1}{k_9} K_8 + \frac{1}{k_{10}} K_9 + \frac{1}{k_{11}} K_{10}\right)$$

$$E = \frac{4k_1}{K_{12}^{3/2}} \left(\frac{1}{k_{10}} K_8 K_9 + \frac{1}{k_{11}} K_9 K_{10}\right)$$

$$F = \frac{4k_1}{K_{12}^{2}} \left(\frac{1}{k_{11} K_8 K_9 K_{10}}\right)$$

A plot of this equation for the experimental data is shown in Figure 6. The least square lines are given below.

Table 10. Least square lines for Figure 6. Isobutane order hydrogenolysis rate data

$\sqrt{\frac{P_{C_4H_{10}}}{R}} = 115.18\ P_{C_4H_{10}} + 8.59$	$P_{H_2} = .45$ torr
$\sqrt{\frac{P_{C_4H_{10}}}{R}} = 29.42\ P_{C_4H_{10}} + 10.68$	$P_{H_2} = 2.03$ torr
$\sqrt{\frac{P_{C_4H_{10}}}{R}} = 13.64\ P_{C_4H_{10}} + 11.12$	$P_{H_2} = 4.20$ torr

Only a few points are shown in Figure 6 for the P_{H_2} = 2.03 and 4.20 torr lines; however, a complete tabulation of data points for all calculations is given in Appendix 1.

The intercepts in these plots should satisfy:

$$I = \frac{B}{A^{\frac{1}{2}}} P_{H_2} + \frac{1}{A^{\frac{1}{2}}}$$

Figure 6. The linearized rate expression at 209°C

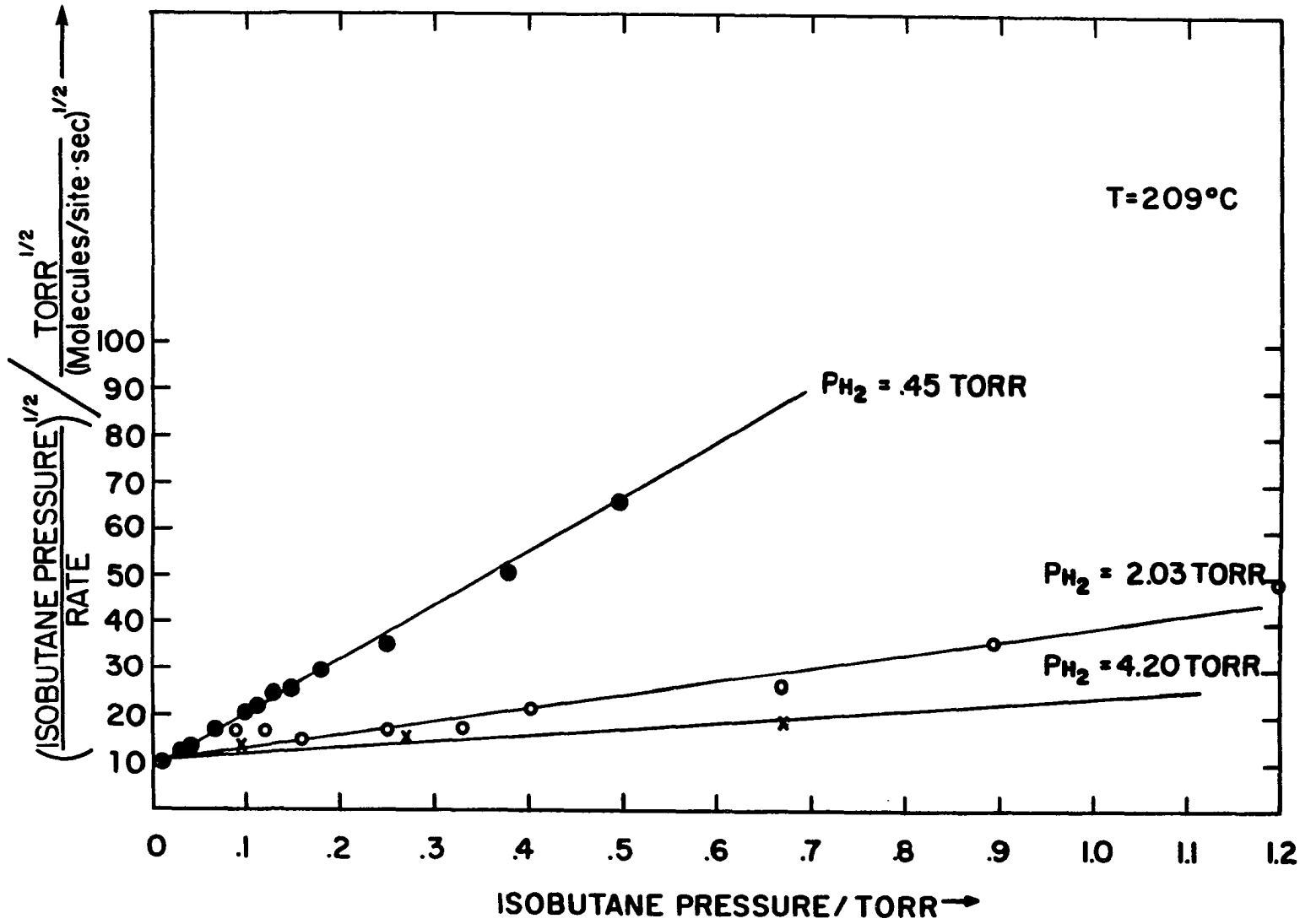
$\left(\frac{\text{ISOBUTANE PRESSURE}}{\text{RATE}}\right)^{1/2} \Big/ \frac{\text{TORR}^{1/2}}{(\text{Molecules/site·sec})^{1/2}}$
T=209°C
P_{H_2} = .45 TORR
P_{H_2} = 2.03 TORR
P_{H_2} = 4.20 TORR
100
90
80
70
60
50
40
30
20
10
0
.1
.2
.3
.4
.5
.6
.7
.8
.9
1.0
1.1
1.2
ISOBUTANE PRESSURE / TORR

yielding another linear graph. Figure 7 shows that a plot of Ivs P_{H_2} derived from the three isobutane order plots in Figure 6 can be reasonably treated as linear, with the best least squares fit given by:

$$I = 1.87\ P_{H_2}^{\frac{1}{2}} + 7.55.$$

This gives the constants A and B in the original rate expression.

$$A = 1.75 \times 10^{-2} \text{ molecules/site} \cdot \text{sec} \cdot \text{torr}$$

$$B = .25\ \text{torr}^{-\frac{1}{2}}$$

Additional information can be obtained from the dependence of the slope of the linearized rate equation on hydrogen pressure. Residue deuteration experiments described earlier, in which the principle product was CH_2D_2, imply that concentrations of C*, and CH* species in the residue were negligible. This implies that the terms E and F in the rate expression are also very small.

It is also found (as will be discussed more fully later) that the kinetic order in hydrogen pressure of the isobutane hydrogenolysis reaction varies from +2 to -1, as the hydrogen pressure increases. This also suggests that the terms E and F are negligible. Neglecting these terms, the slope of the linearized rate low plot is:

$$S = \frac{1}{A^{\frac{1}{2}}}\left[\frac{C}{P_{H_2}^{\frac{1}{2}}} + \frac{D}{P_{H_2}} + \frac{E}{P_{H_2}^{3/2}} + \frac{F}{P_{H_2}^{2}}\right] = \frac{1}{A^{\frac{1}{2}}}\left[\frac{C}{P_{H_2}^{\frac{1}{2}}} + \frac{D}{P_{H_2}}\right].$$

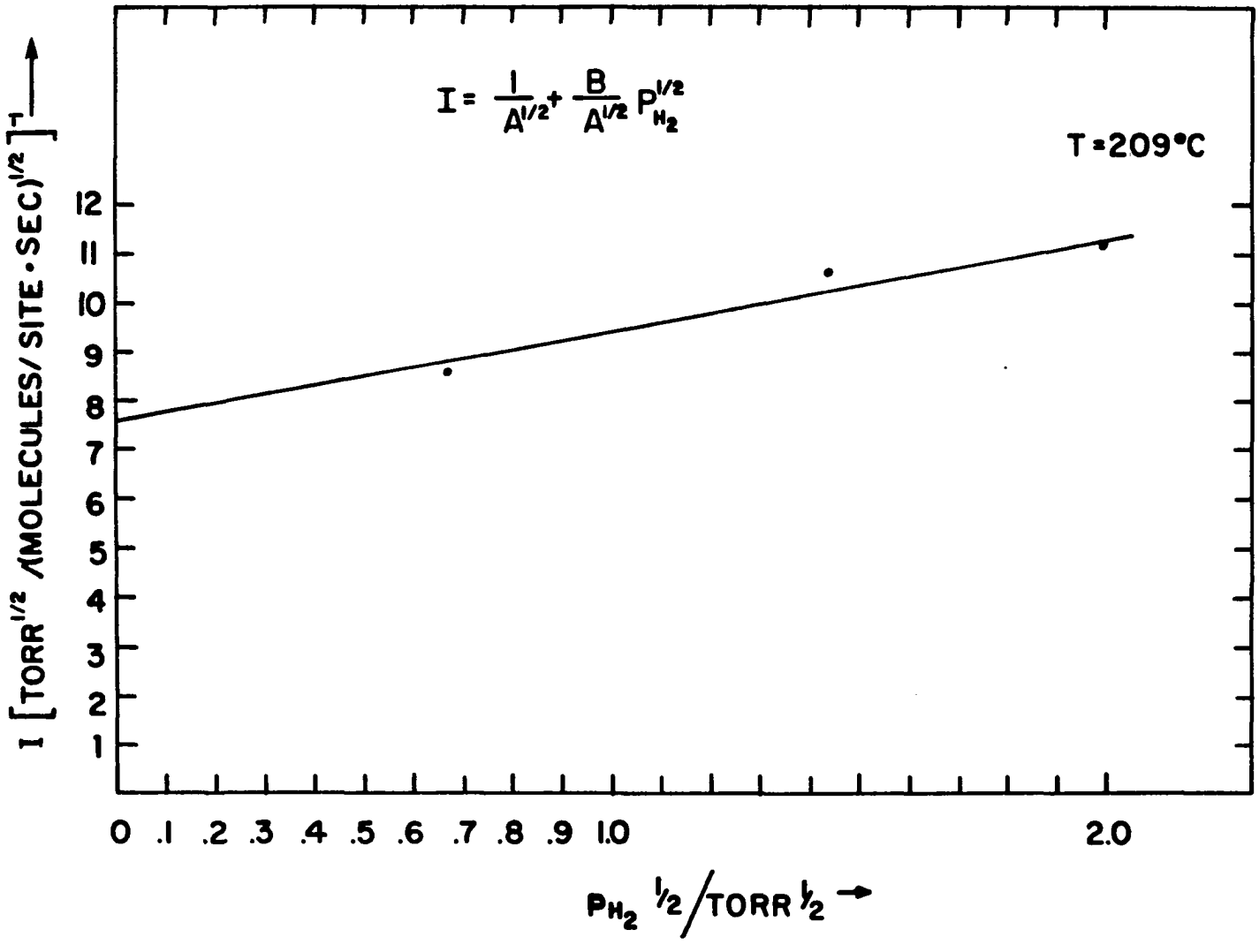

Figure 7. The intercept of the linearized rate law as a function of hydrogen at 209°C

Multiplying through by $P_{H_2}^{\frac{1}{2}}$ gives

$$P_{H_2}^{\frac{1}{2}} S = \frac{D}{A^{\frac{1}{2}}} P_{H_2}^{-\frac{1}{2}} + \frac{C}{A^{\frac{1}{2}}}$$

Figure 8 is a plot of $P_{H_2}^{\frac{1}{2}} S$ vs $P_{H_2}^{-\frac{1}{2}}$. The least squares slope and intercept can be used to solve for C and D.

$$P_{H_2}^{-\frac{1}{2}} S = \frac{48.02}{P_{H_2}^{\frac{1}{2}}} + 6.17$$

$$C = .81 \text{ torr}^{-\frac{1}{2}}$$

$$D = 6.34 \text{ (dimensionless)}$$

The rate expression can now be stated as follows.

$$R = \frac{1.75 \times 10^{-2} \frac{\text{molecules}}{\text{site sec torr}} P_{C_4H_{10}}}{\left[1 + .25 \text{ torr}^{-\frac{1}{2}} P_{H_2}^{\frac{1}{2}} + \frac{.81 \text{ torr}^{-\frac{1}{2}} P_{C_4H_{10}}}{P_{H_2}^{\frac{1}{2}}} + \frac{6.34 P_{C_4H_{10}}}{P_{H_2}}\right]^2}$$

Theoretical fits to the experimental data are shown in Figures 9 through 12.

The isobutane order varies from +1 to -1 while the hydrogen order varies from +2 to -1. The +2 order exhibited at low hydrogen pressure (isobutane pressure held constant) indicates that the D term in the demoninator dominates in the pressure regime over which data have been

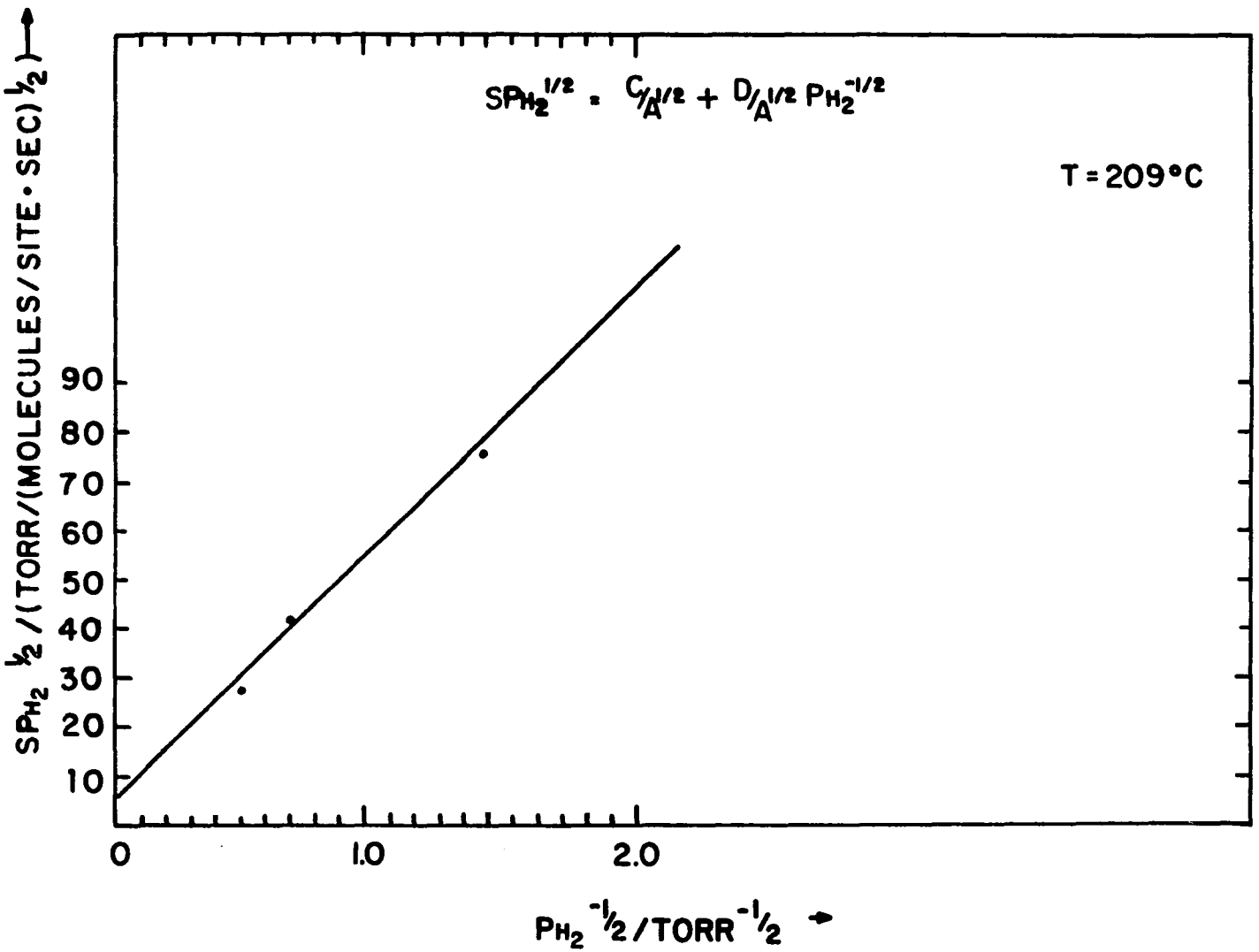

Figure 8. The slopes of the linearized rate law as a function of hydrogen pressure

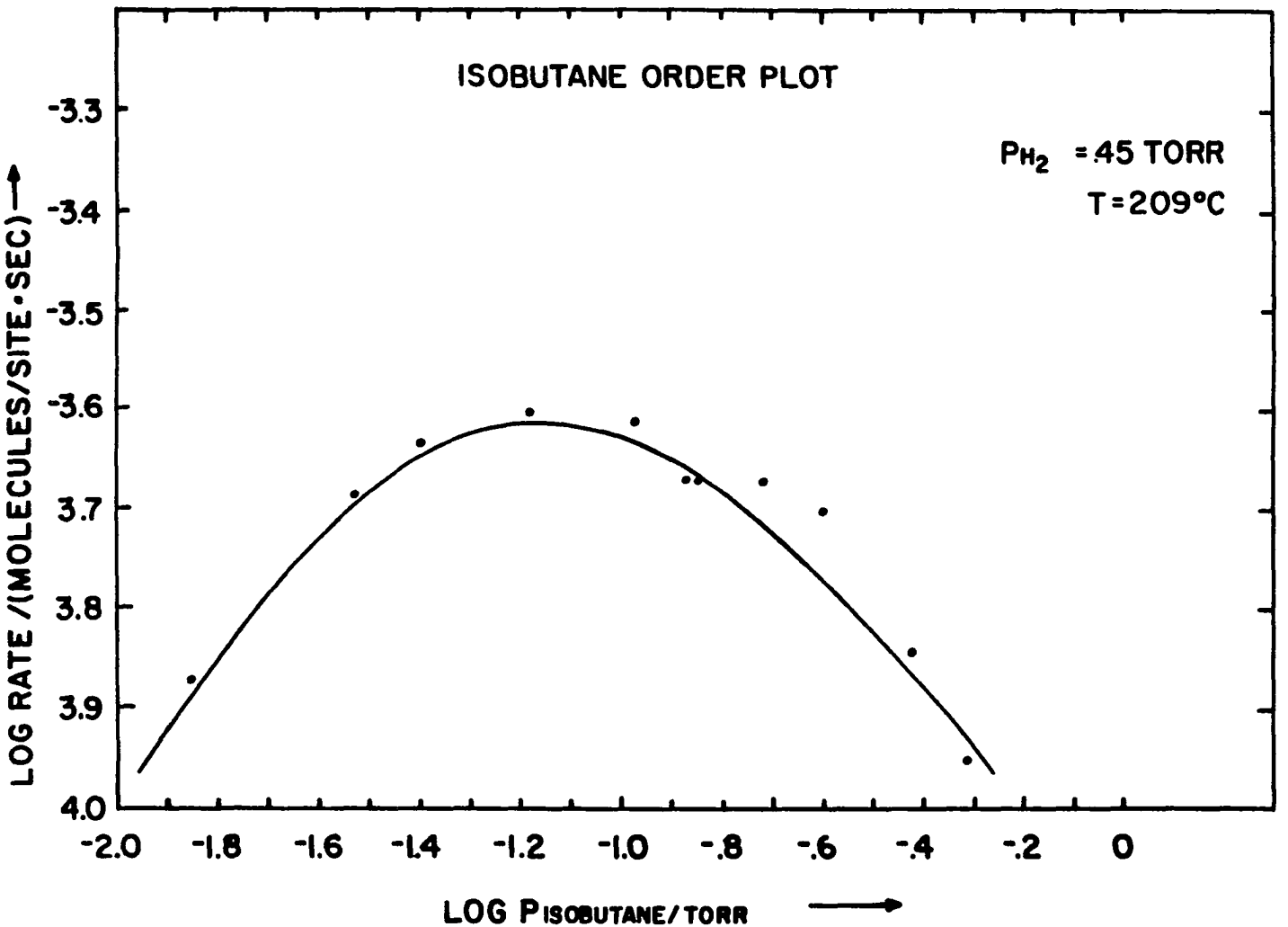

Figure 9. Hydrogenolysis reaction kinetic data at 209°C

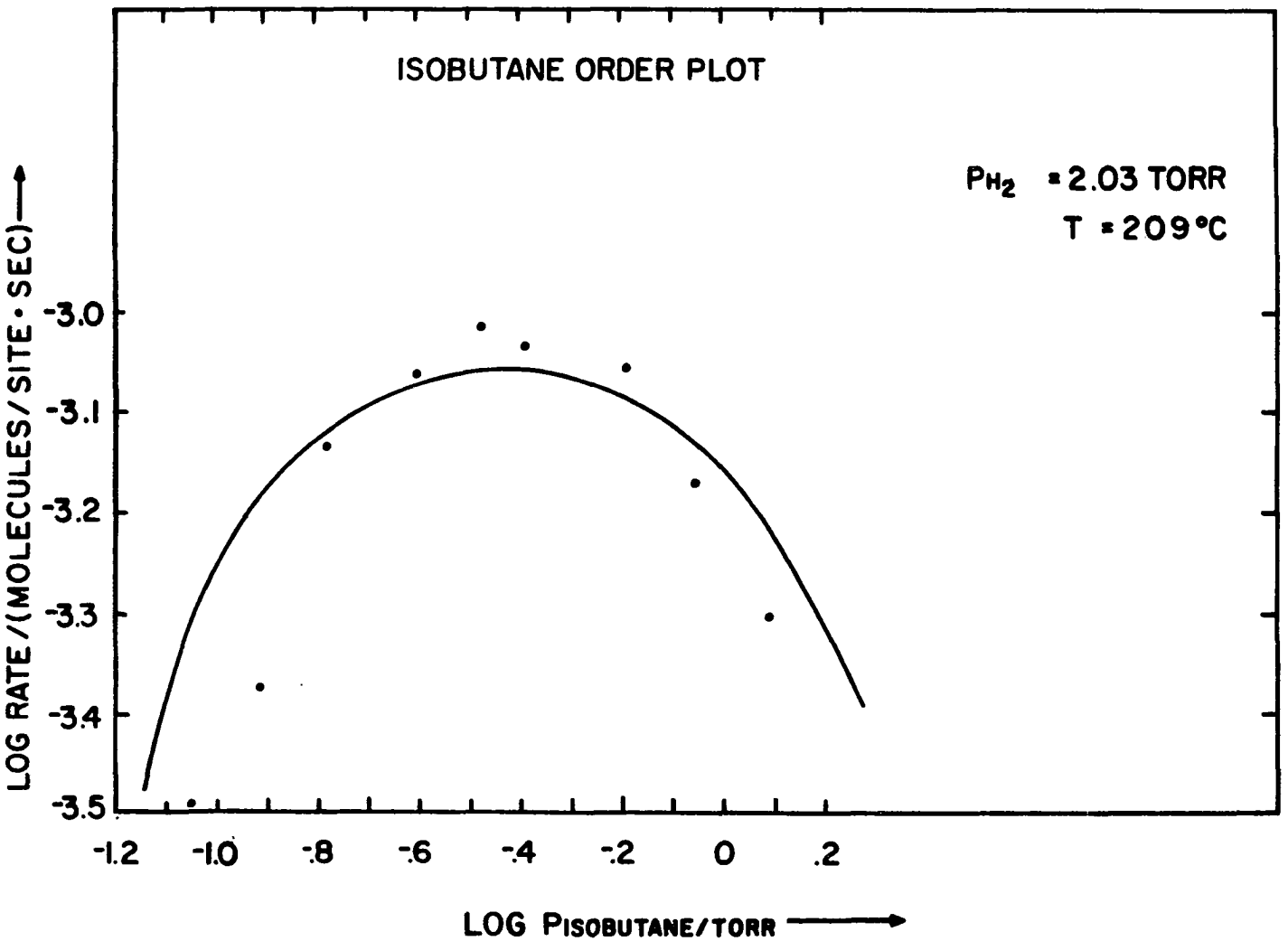

Figure 10. Hydrogenolysis reaction kinetic data at 209°C

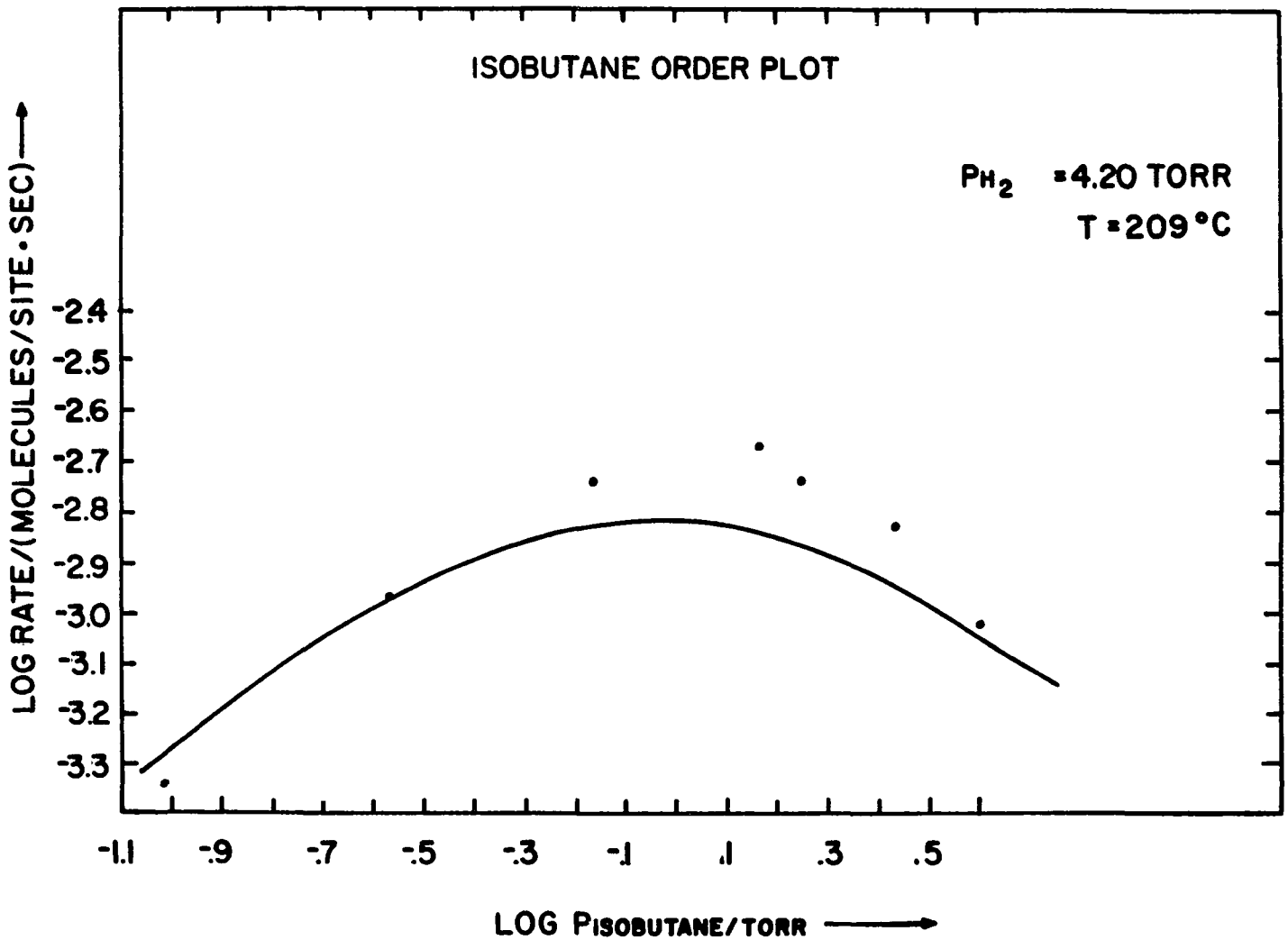

Figure 11. Hydrogenolysis reaction kinetic data at 209°C

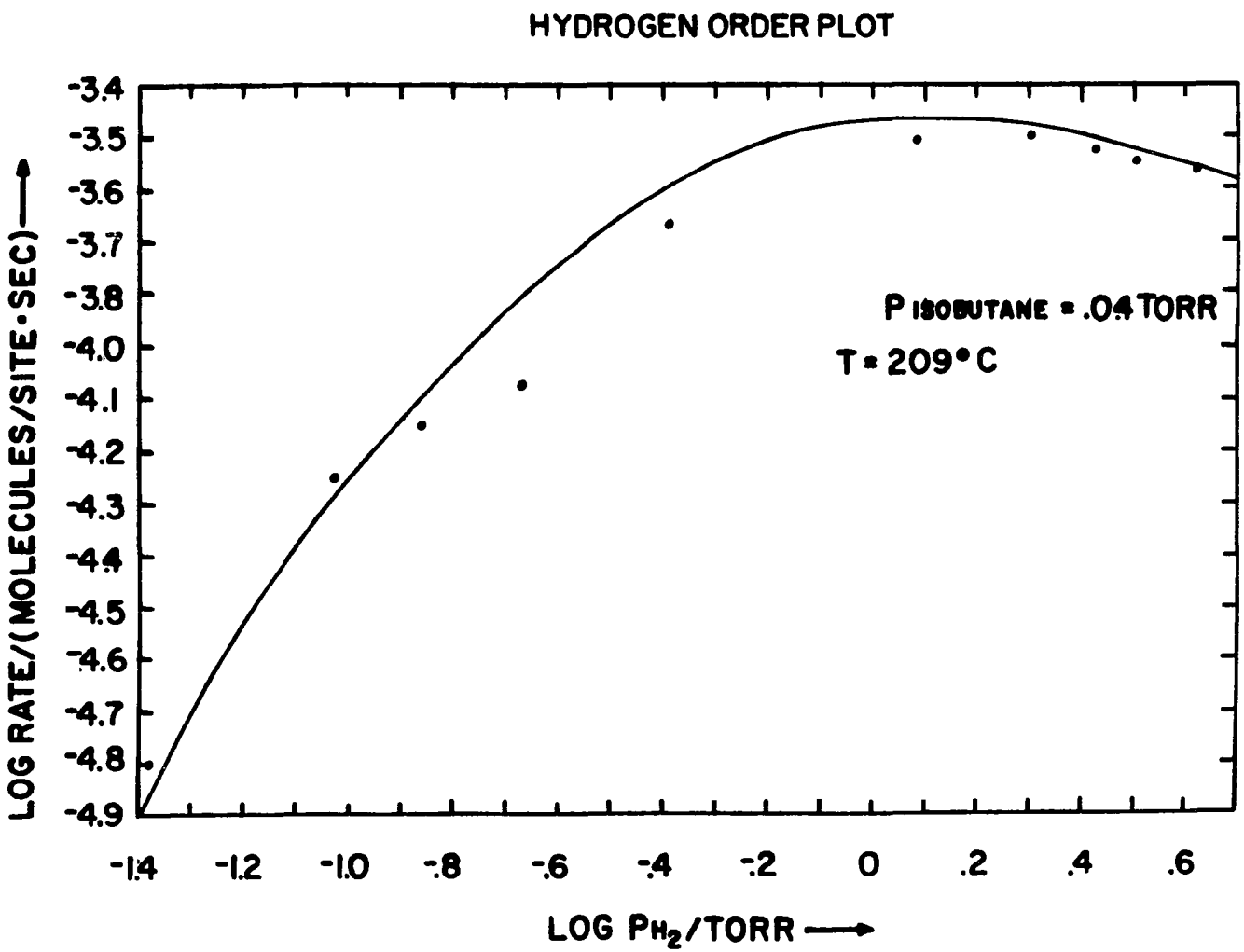

Figure 12. Hydrogenolysis reaction kinetic data at 209°C

taken. The most probable reason for E and F being negligible in the rate expression is k_{-8} and k_{-9} are very small compared to the forward reaction rate constants. If this were not so and reactions 8 through 10 were at equilibrium then as the ambient is pumped out all monocarbon species would go to C* by the Le Chatelier principle. Deuteration would yield only CD_4. This is clearly not the case; CH_2D_2 is the major product of deuteration.

The processes:

$$CH_2^* + * \xrightarrow{k_{-9}} CH^* + H^*$$

$$CH^* + * \xrightarrow{k_{-8}} C^* + H^*$$

being negligible, steps 8 and 9 must be essentially irreversible. Now the elementary reactions for isobutane hydrogenolysis between 175°C and 209°C can be written as shown below.

$$C_4H_{10}(g) + 2^* \xrightarrow{k_1} C_4H_9^* + H^*$$

$$C_4H_9^* + * \xrightarrow{k_2} C_4H_8^* + H^*$$

$$C_4H_8^* + * \xrightarrow{k_3} C_3H_6^* + CH_2^*$$

$$C_3H_6^* + * \xrightarrow{k_4} C_3H_5^* + H^*$$

$$C_3H_5^* + * \xrightarrow{k_5} C_2H_3^* + CH_2^*$$

$$C_2H_3^* + * \xrightarrow{k_6} C_2H_2^* + H^*$$

$$C_2H_2^* + * \xrightarrow{k_7} C^* + CH_2^*$$

$$C^* + H^* \xrightarrow{k_8} CH^* + *$$

$$CH^* + H^* \xrightarrow{k_9} CH_2^* + *$$

$$CH_2^* + H^* \underset{k_{-10}}{\overset{k_{10}}{\rightleftharpoons}} CH_3^* + *$$

$$CH_3^* + H^* \xrightarrow{k_{11}} CH_4(g) + 2^*$$

$$H_2(g) + 2^* \underset{k_{-12}}{\overset{k_{12}}{\rightleftharpoons}} 2H^*$$

Since the rate expression is much less complex than the one initially derived, a number of individual rate constants can be obtained. These constants are (at 209°C):

$$A = 4k_1 = 1.75 \times 10^{-2} \text{ molecules/site} \cdot \text{sec} \cdot \text{torr}$$

$$B = K_{12}^{\frac{1}{2}} = .25 \text{ torr}^{-\frac{1}{2}}$$

The major surface species is CH_2^*, therefore:

$$C = 4k_1/\sqrt{K_{12}}\, k_{10} = .81 \text{ torr}^{-\frac{1}{2}}$$

$$D = \frac{4k_1}{k_{11} K_{10} K_{12}} = 6.34 \text{ (dimensionless)}$$

$$k_{10} = 8.65 \times 10^{-2} \text{ molecules/site} \cdot \text{sec}$$

$$k_{11} K_{10} = 4.60 \times 10^{-3} \text{ molecules/site} \cdot \text{sec}$$

The hydrogen order variation observed here (+2 to -1) has also been observed for ethane on iridium and platinum (22,42). The hydrogen adsorption equilibrium constant K_{12} was found to be lower in this study than in previous investigations (22,28) on iridium, however, most of these studies were conducted at lower temperatures. Therefore, rate data were obtained at a lower temperature in an attempt to elucidate the temperature dependence of the hydrogen adsorption equilibrium constant. Single crystal studies on iridium show that hydrocarbon surface coverage increases with increasing temperature while hydrogen coverage decreases (38). The number of active sites had to be recalculated since it was expected that hydrocarbon surface coverage would be different at a lower reaction temperature. Figures 13 and 14 are methane desorption curves at 175°C. The maximum number of surface sites available at 175°C (assuming a one-to-one correspondence between surface carbon and active site) is:

$$n_{MAX}(175°C) = 6.70 \times 10^{16} \text{ sites}$$

Comparing this value to the one previously determined at 209°C [$n_{MAX}(209°C) = 20.00 \times 10^{16}$ sites], it is apparent that hydrocarbon sur-

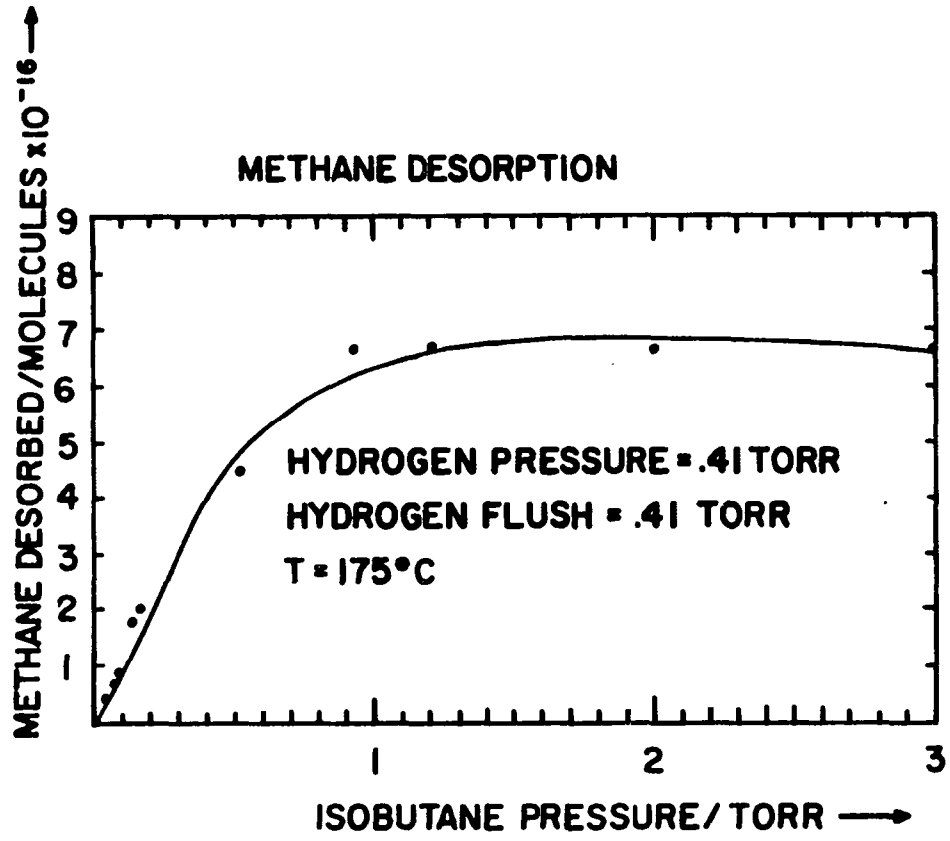

Figure 13. Methane desorption as a function of isobutane pressure at 175°C

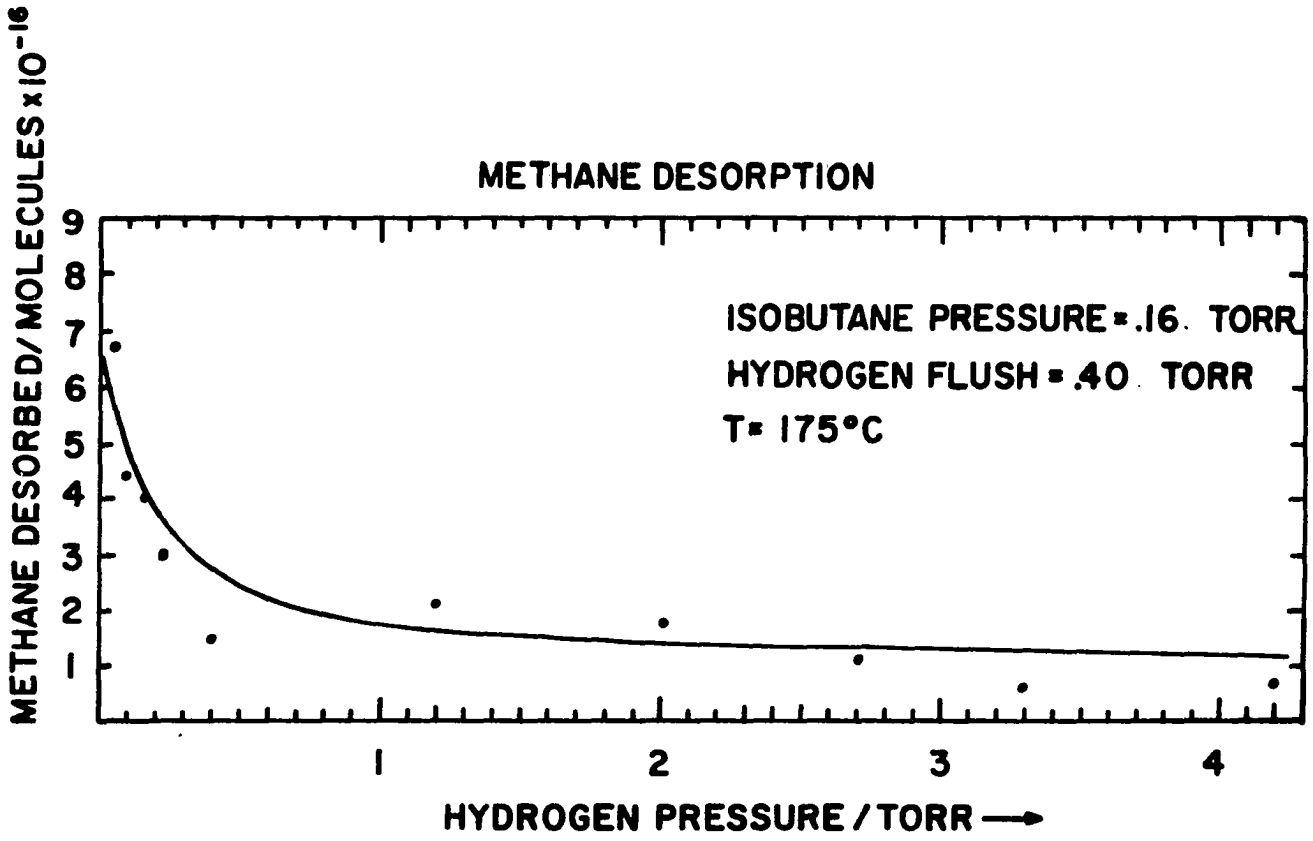

Figure 14. Methane desorption as a function of hydrogen pressure at 175°C

face coverage does increase as temperature increases. Making a linear plot for the isobutane order data yields the following least squares fit.

$$\sqrt{\frac{P_{C_4H_{10}}}{R}} = 12.35\ P_{C_4H_{10}} + 40.09$$

$$\frac{1 + B\ P_{H_2}}{A^{\frac{1}{2}}} = 40.09 \qquad \frac{D}{A^{\frac{1}{2}}\ P_{H_2}} = 12.35$$

This graph is shown in Figure 15.

Preliminary curve fitting of the hydrogen order data gave the constant B.

$$B = 1.9\ \text{torr}^{-\frac{1}{2}}$$

The constants A and D can now be calculated and are shown below.

$$A = 1.46 \times 10^{-2}\ \text{molecules/site} \cdot \text{sec} \cdot \text{torr}$$

$$D = 6.12\ \text{(dimensionless)}$$

The value of C used in the 209°C fit was tried for the 175°C data as an initial guess, however, it fit the data quite well.

$$C = .81\ \text{torr}^{-\frac{1}{2}}$$

Figures 16 and 17 show the theoretical fit to the experimental data at 175°C. The rate expression at 175°C is:

Figure 15. Linearized rate law at 175°C

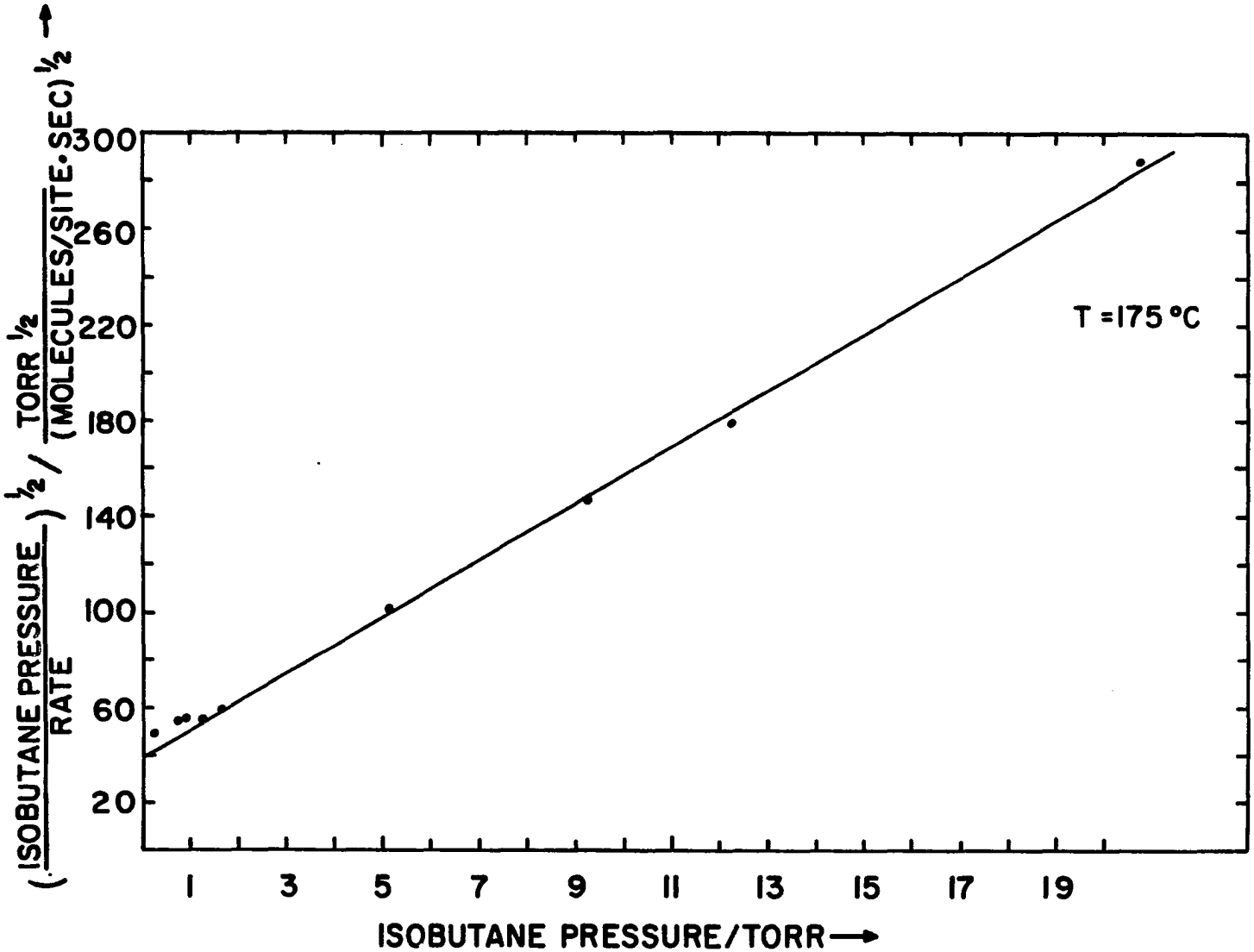
$\left(\frac{\text{ISOBUTANE PRESSURE}}{\text{RATE}}\right)^{1/2} / \frac{\text{TORR}^{1/2}}{(\text{MOLECULES/SITE}\cdot\text{SEC})^{1/2}} \rightarrow$
300
260
220
180
140
100
60
20
T = 175 °C
1
3
5
7
9
11
13
15
17
19
ISOBUTANE PRESSURE/TORR ⟶

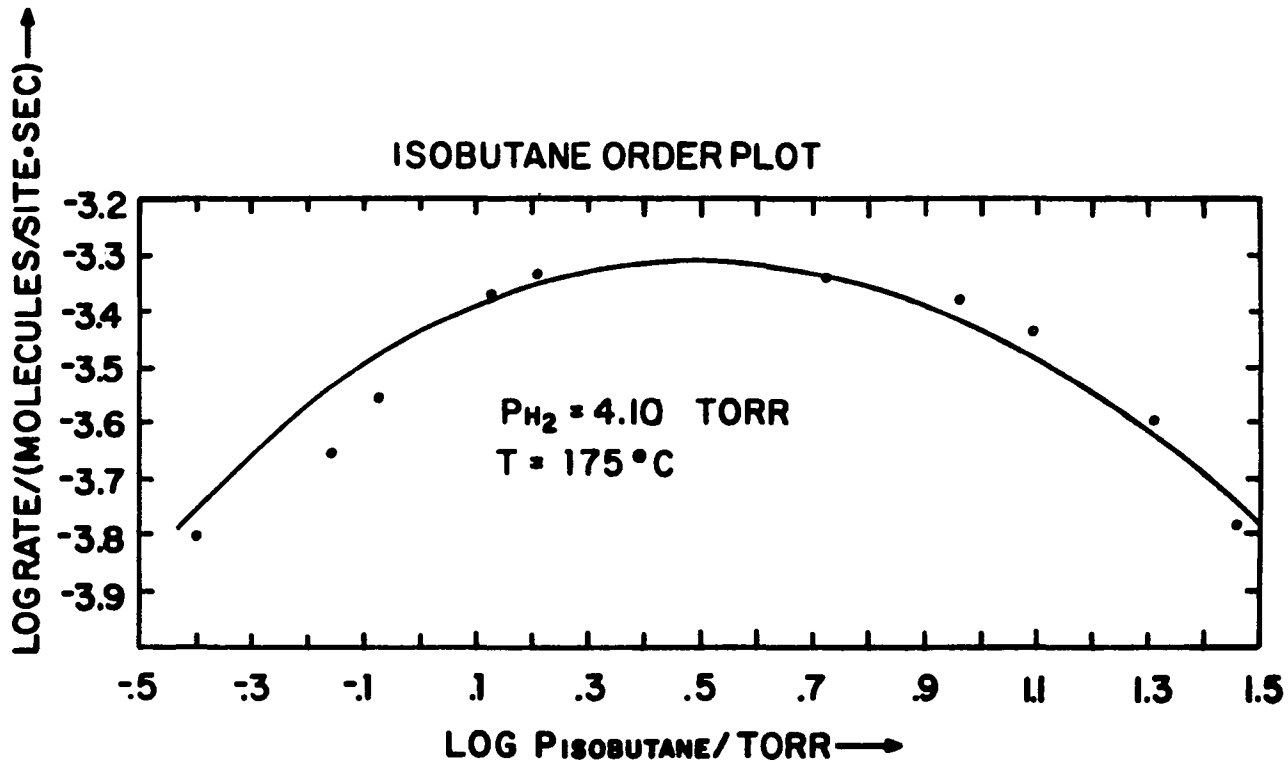

Figure 16. Hydrogenolysis reaction kinetic data at 175°C

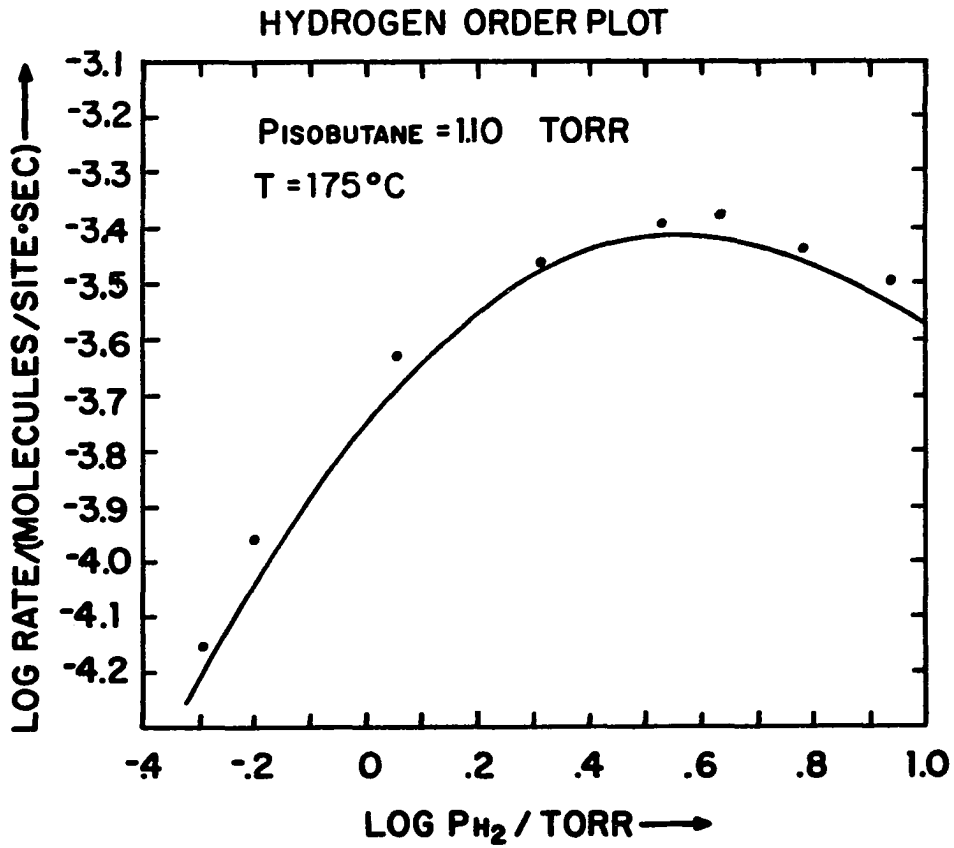

Figure 17. Hydrogenolysis reaction kinetic data at 175°C

$$R = \frac{1.46 \times 10^{-2} \text{ molecules/site} \cdot \text{sec} \cdot \text{torr} \; P_{C_4H_{10}}}{\left[1 + 1.9 \text{ torr}^{-\frac{1}{2}} P_{H_2} + \frac{.81 \text{ torr}^{-\frac{1}{2}} P_{C_4H_{10}}}{P_{H_2}^{\frac{1}{2}}} + \frac{6.12 P_{C_4H_{10}}}{P_{H_2}}\right]^2}$$

The hydrogen adsorption equilibrium constant decreases as temperature increases [K_{12} (209°C) = .06 torr^{-1}, K_{12} (175°C) = 3.61 torr^{-1}). Therefore, more hydrocarbon is on the surface at 209°C than at 175°C (P_{H_2} = constant). The following figure shows the surface coverage of monocarbon fragments as a function of temperature (P_{H_2} and $P_{C_4H_{10}}$ constant). At low temperatures, hydrocarbon coverage in the form of monocarbon fragments is low while hydrogen coverage is high and polycarbon surface fragments are reversibly adsorbed to the surface. As the temperature increases, hydrogen surface coverage decreases (K_{12} decreases) and polycarbon surface species which are reversibly adsorbed start decomposing into monocarbon fragments. As mentioned earlier, it was shown that at low temperatures (100°C) deuterium exchange occurs for hydrocarbons on iridium but as temperature increases, hydrogenolysis becomes the predominant reaction. These reversibly adsorbed hydrocarbons retain their gas phase carbon skeletal features and prefer exchange to hydrogenolysis at low temperatures. Acting as poisons, they take up sites on the surface that would have been available for monocarbon species. Eventually, Figure 18 will level off in the high temperature limit. The surface will be covered by a carbonaceous monolayer.

When saturation occurs, only monocarbon fragments will be on the sur-

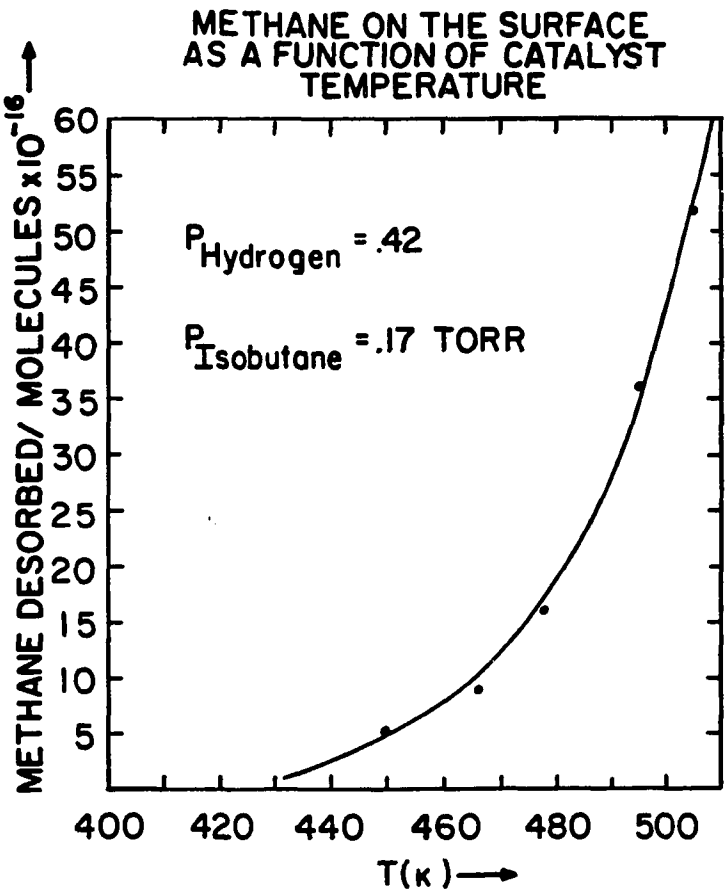

Figure 18. Adsorption as a function of temperature

face and no hydrogen will be adsorbed. If the rate of hydrogenolysis is still significant at this point (temperature that causes leveling off in Figure 18), then a Rideal-Eley mechanism must be operating in this region. There is the possibility that at low temperatures a Langmuir-Hinshelwood mechanism dominates while at high temperatures a Rideal-Eley model accounts for hydrogenolysis. At lower temperatures, isomerization may also become a significant reaction, since carbon skeletal degradation will occur to a lesser extent. This would also account for the decrease in the number of monocarbon fragments on the surface at low temperatures. The reverse rate constants for elementary reactions one and two must also become larger as temperature is decreased. Only monocarbon fragments are observed after pumpout during hydrogenation. According to the law of mass action, decreasing the isobutane pressure during pumping causes more reversibly adsorbed hydrocarbon to desorb at lower temperatures.

The geometric surface area of the glass bulb reaction flask containing the catalyst is 303.62 cm^2. The surface area occupied by one methane molecule is approximately 6.92×10^{-16} cm^2 (CH_4 van der Waals radius = 1.485 Å). The following table shows how many metal atoms are involved in the active site based on the geometric surface area of the catalyst.

Table 11. Metal atoms involved in the active site

T°C	Surface area occupied	$\frac{\text{Geometric area}}{\text{Area occupied}} = \frac{\text{\# metal}}{\text{site}}$
175	45.43 cm^2	7
209	135.60 cm^2	2
237	355.96 cm^2	1

The actual surface area of the catalyst is greater than the geometric surface area in general. Therefore, the above values should only be regarded as approximate determinations. The values in Table 11 are plausible. As many as 12 metal atoms have been proposed to be associated with the active site for ethane hydrogenolysis on nickel (43). The curve in Figure 18 most probably will start leveling off above 237°C (510K). Higher temperature data could not be obtained due to experimental limitations, however, this is an interesting area for future investigation.

There are a number of reasons why the number of metal atoms per active site can vary with temperature. One explanation is the major surface species changes as a function of temperature. An example of this is shown below:

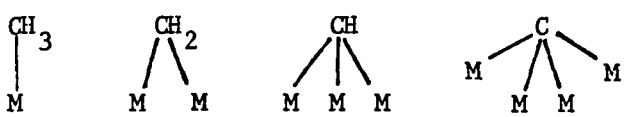

Another possibility is the surface species bonding changes due to structural changes in the catalyst surface (reconstruction).

Reversibly adsorbed hydrocarbon (significant at lower temperatures) can account for some metal atoms being used for adsorption sites. Increased adsorbate mobility would also account for more metal atoms being involved

in an adsorption site due to delocalization of the adsorbate. Hydrogen adsorption can also reduce the number of sites available for hydrocarbon adsorption. This would increase the metal atom to carbon atom ratio as temperature decreases.

The hydrogen surface concentration can be expressed in terms of its equilibrium constant.

$$K_{12} = \frac{(H^*)^2}{P_{H_2}(*)}$$

Using the expression derived for (*) gives:

$$(H^*) = \theta_{hydrogen} = \frac{\sqrt{K_{12}}\, P_{H_2}^{\frac{1}{2}}}{1 + \sqrt{K_{12}}\, P_{H_2}^{\frac{1}{2}} + \frac{k_1 \; P_{C_4H_{10}}}{k_{10}\sqrt{K_{12}}\, P_{H_2}^{\frac{1}{2}}} + \frac{4k_1}{k_{11} K_{10} K_{12}} \frac{P_{C_4H_{10}}}{P_{H_2}}}$$

At 175°C, the hydrogen coverage is given below for $P_{C_4H_{10}} = .17$ torr and $P_{H_2} = .42$ torr.

$$\theta_{hydrogen} = \frac{1.90(.42)^{\frac{1}{2}}}{1 + 1.9(.42)^{\frac{1}{2}} + \frac{.81(.17)}{(.42)^{\frac{1}{2}}} + \frac{6.12(.17)}{.42}}$$

$$\theta_{hydrogen} = .25$$

At 209°C, the hydrogen coverage is:

$$\theta_{hydrogen} = .04$$

It appears that hydrogen adsorption is also partially responsible for the variation in the metal to carbon surface ratio. If hydrocarbon coverage increases significantly above 510K, there will be 2 or more carbons associated with each metal surface atom. This could occur if the carbonaceous layer was in the form of irreversibly bound ethylidene.

An energy of activation analysis is shown in Figure 19. The apparent activation energy is 24.20 kcal/mole. This value is intermediate to values of the energy of activation for ethane hydrogenolysis, 25.5 kcal per mole (22) and neopentane hydrogenolysis, 17.5 kcal/mole (28) on iridium thin films. It appears that while the initial points of attachment to the surface of hydrocarbons on iridium may be different, the mechanisms of hydrogenolysis are essentially the same. Hydrocarbons tend to decompose as fast as possible on the iridium surface at temperatures above about 170°C, into monocarbon surface fragments. This irreversible decomposition into monocarbon surface intermediates accounts for methane being the sole product of hydrogenolysis.

Table 12 gives the individual rate constants at 175°C and 209°C.

Table 12. Some hydrogenolysis rate constants

T°C	k_1 (molecules/site•sec•torr)	K_{12} ($torr^{-1}$)	k_{10} (molecules/site•sec)
175	$.36 \times 10^{-2}$	3.61	$.95 \times 10^{-2}$
209	$.44 \times 10^{-2}$	.06	8.65×10^{-2}

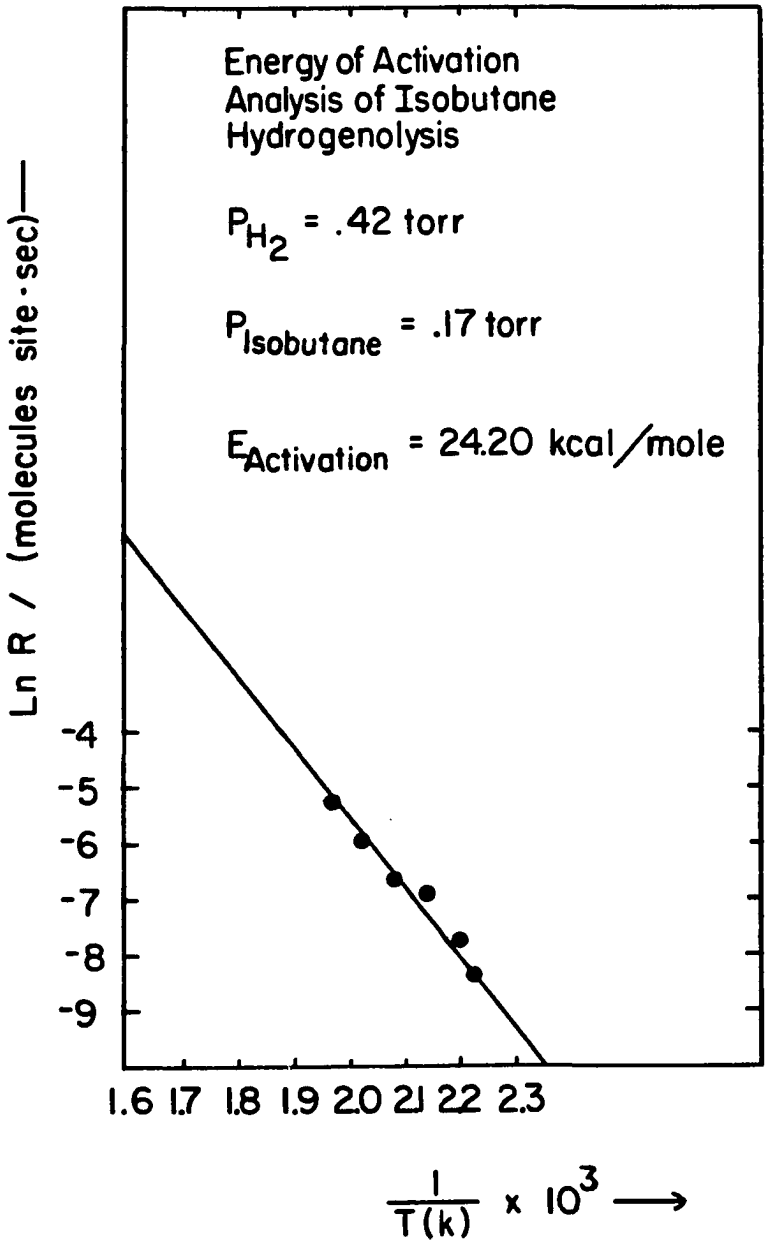

Figure 19. Energy of activation analysis

In general, for any rate constant:

$$k_i = Ae^{-E_i/RT}$$

$$E_i = -R \ln \frac{k_i(T_2)}{k_i(T_1)} \quad \frac{T_1T_2}{T_1 - T_2}$$

The energy of dissociative hydrocarbon adsorption (elementary step 1) can be calculated.

$$E_{adsorption}\ (k_1) = 2.52 \text{ kcal/mole}$$

Since $E_{desorption} - E_{adsorption} = \Delta H$ (ΔH = enthalpy change during dissociative hydrocarbon adsorption) and $\Delta H = E_{H-Ir} + E_{C-Ir} - E_{C-H}$ for elementary reaction step 1, $E_{desorption}$ must be very high compared to adsorption ($E_{Ir-H} + E_{Ir-C} - E_{CH}$ on the order of 60 kcal/mole). Therefore, energy considerations favor adsorption and dissociation of the hydrocarbon as opposed to reversible adsorption with carbon skeleton retention.

The enthalpy of hydrogen adsorption can also be calculated.

$$\Delta H(K_{12}) = 51.52 \text{ kcal/mole}$$

This value is higher than values reported in the literature by about 21 kcal/mole (44), however, it is assumed here that the enthalpy of adsorption is not a function of surface coverage and in all probability it is. Heats of reaction are also a function of the support used (energies of activation can vary by 20 kcal/mole for different supports). Here, the catalyst is vapor deposited on pyrex.

The activation energy for the net hydrogenolysis of isobutane is intermediate to those determined for ethane and neopentane. Since neopentane can't 1,2 diadsorb and ethane can't 1,3 diadsorb or triadsorb, isobutane must be adsorbing in all three fashions (1,2; 1,3 diadsorption and triadsorption), however, between 175°C to 200°C decomposition into monocarbon fragments is extremely rapid. Very little isobutane remains on the surface with its carbon skeleton intact.

Mechanistic Interpretation

An evaporated iridium thin film is polycrystalline. It consists of the low indexed (100), (110) and (111) surfaces as well as surface steps, kinks and other high indexed planes. Although some work has been done on inducing film orientation in general, films will exhibit all the characteristic features described above. It has been found that the (110) iridium surface reconstructs to a 1 x 2 surface arrangement when cleaned (45, 46). Hydrocarbon adsorption as well as oxygen adsorption transforms the (1 x 2) structure to a (1 x 1) surface (45,46). The clean Ir (111) surface retains its f.c.c. arrangement at the surface as does the (100) crystal plane (47,48). Hydrocarbon adsorption to the (111) surface produces a (9 x 9) surface structure while adsorption to the Ir (100) surface produces a (1 x 1) and a (5 x 1) overlayer (48). Stepped iridium surfaces have been found to exhibit disordered carbonaceous overlayers (34). Hydrogen adsorption does not alter the LEED patterns of the (110), (100), (111) or stepped iridium surfaces (38). Since hydrogen and hydrocarbon

fragments are bound more strongly to stepped surfaces than low indexed planes, it is believed that hydrogenolysis occurs on high indexed surfaces as well as on the (110) (1 x 2) reconstructed surface. The (110) surface is believed to behave as a stepped surface since it can be envisioned as a surface composed of monoatomic height (111) steps separated by "terraces" one atom in width. Single crystal studies (38) show hydrocarbon surface coverage increases while hydrogen surface coverage decreases as temperature increases; this is in agreement with (Figure 18 in this thesis) polycrystalline results. It appears the hydrogen is extremely mobile on the metal surface since diffusion energies are much lower than desorption energies for hydrogen on iridium (48,49). It has been postulated that the energy of activation necessary for hydrogen diffusion increases near high indexed planes and steps, thus making hydrogen appear to be held more strongly at these locations.

The following reaction sequence is a possible explanation of carbon bond scission on the surface. These reactions parallel the previous sequence of reactions used to derive the kinetic rate law. The isobutane molecule must break down completely into monocarbon fragments rapidly since no lower hydrocarbon fragments are observed except methane. The (110) surface is used here since it is not smooth and is the most probable low index site for hydrogenolysis. This surface is shown on the next page. Isobutane chemisorption and carbon carbon bond scission are shown in the next figure. The hydrogens fall into the troughs where they can linearly diffuse across the surface while the CH_2 fragments remain

CLEAN IR (110)-(1X2) RECONSTRUCTED SURFACE

TOP VIEW

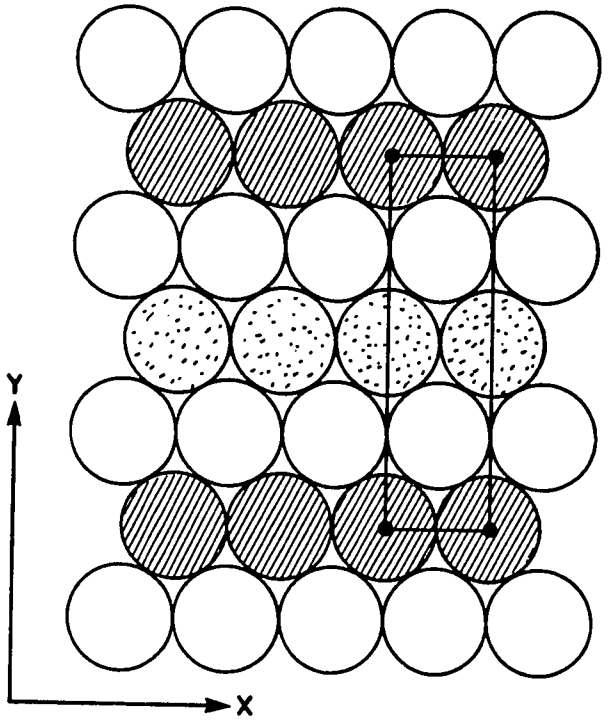

SIDE VIEW

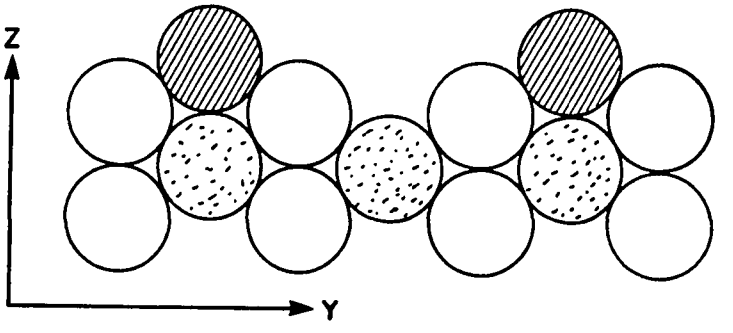

Figure 20. Ir (1 x 2) surface

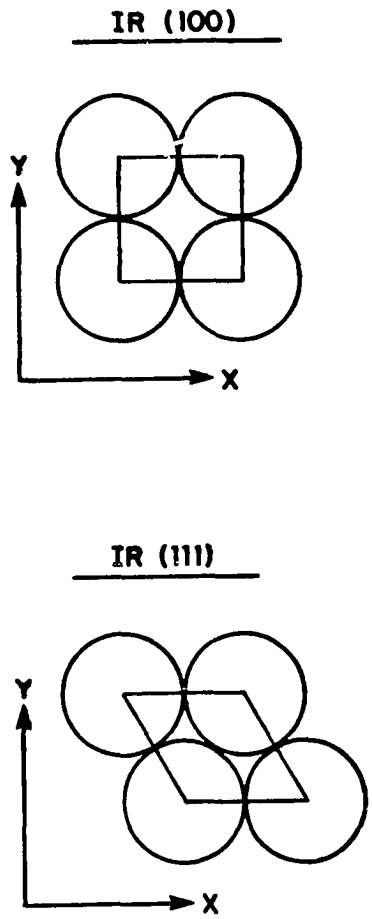

Figure 21. The Ir (111) and (100) surfaces

CHEMISORPTION AND DECOMPOSITION
OF ISOBUTANE

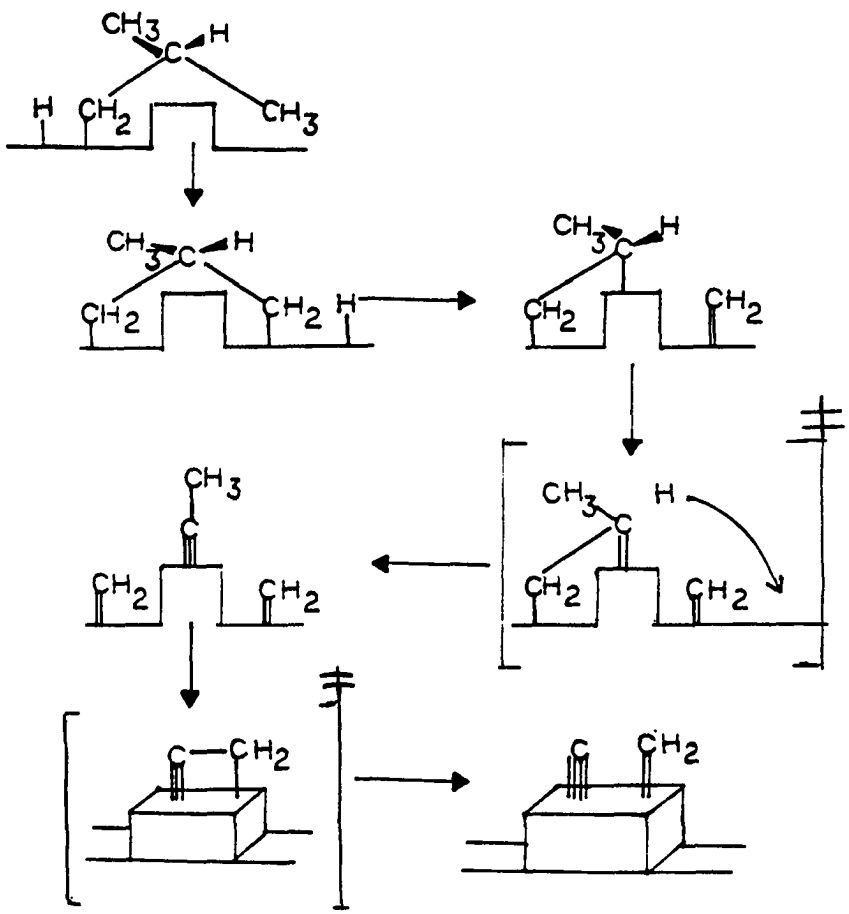

Figure 22. Isobutane adsorption

fixed to the active site. Hydrogenation of the monocarbon fragments is followed by methane desorption to complete the process.

Hydrogenolysis activity has been linked to the percent d character of the metal bond (19,21), however, it is more physically significant to discuss this effect in terms of d orbital occupancy. As d orbital occupancy is decreased, hydrogenolysis activity of the metals goes through a maximum, for example:

Metal	Re	Os	Ir	Pt
Relative activity for ethane hydrogenolysis at 250°C	10^6	10^8	10^6	1

from Sinfelt (21)

This can be explained on the basis of chemisorption of the reactant hydrocarbon. As d orbital occupancy decreases, the electron deficient d orbitals chemisorb hydrocarbon free radicals more readily. Increasing the surface concentration of hydrocarbon increases the rate of hydrogenolysis. However, at very low orbital occupancy, the hydrocarbon is bound to the metal surface too strongly to react with hydrogen and desorb, so hydrogenolysis activity decreases. Alloying can be used to regulate the contents of the metal surface.

By increasing or decreasing the amounts of various metals in the alloy surface, the catalytic activity of the alloy can be regulated (23).

Surface contamination plays an extremely important role in catalysis.

Reactant chemisorption is a prerequisite for hydrogenolysis and surface contamination can preclude this process (23). In some reactions, adsorption of species which are seemingly unrelated to the reaction can enhance catalytic activity. An example of this type of behavior is found in the oxidation of ethylene over silver, where preadsorption of small amounts of Cl^- (moderator) increases the yield significantly (50). However, in the hydrogenolysis of hydrocarbons on nickel, oxygen contamination decreases catalytic activity (23).

Summary and Future Research Suggestions

The hydrogenolysis of isobutane has been investigated over the pressure range 0.1-10.0 torr. The iridium catalyst is a 48.5 Å thick film vapor deposited on the inside of a round bottom flask under ultra high vacuum conditions. Methane was observed to be the only product. The net reaction for this process is:

$$C_4H_{10} + 3H_2 = 4CH_4$$

Isobutane hydrogenolysis is accomplished via irreversible adsorption of the hydrocarbon followed by decomposition on the iridium surface into monocarbon fragments. Subsequent hydrogenation and desorption of these monocarbon fragments in the form of methane completes the process. Exchange between deuterium and isobutane is negligible at 175°C and 209°C. Thermal desorption shows isobutane adsorption and decomposition to be irreversible. Thermal desorption distinguishes three binding states for hydrogen on polycrystalline iridium containing carbon. The two states

leading to hydrogen desorption at 110°C and 160°C are due to hydrogen atomically adsorbed on low and high index crystal planes, respectively. Hydrogen desorbing at 320°C is due to hydrogen bound to carbonaceous fragments chemisorbed to the surface.

Hydrocarbon adsorption increases with increasing temperature while hydrogen adsorption decreases. The equilibrium constant for hydrogen adsorption decreases as temperature increases. Catalyst regeneration procedures employing deuterium and reaction order data indicate that CH_2* is the major surface species. Dependence of reaction rate on hydrogen and isobutane partial pressures was established by measurements of initial rates of methane production. The following rate law fit the experimental data very well.

$$R = \frac{A\, P_{C_4H_{10}}}{\left[1 + B\, P_{H_2}^{\frac{1}{2}} + \frac{C}{P_{H_2}^{\frac{1}{2}}} P_{C_4H_{10}} + \frac{D}{P_{H_2}} P_{C_4H_{10}}\right]^2}$$

Hydrogenolysis of isobutane on iridium occurs via a Langmuir Hinshelwood mechanism. The hydrogen order varies from +2 to -1. The isobutane order varies from +1 to -1.

The activation energy for hydrogenolysis is 24.20 kcal/mole. The heat of adsorption of hydrogen on the iridium thin film is 51.52 kcal per mole. The activation energy for hydrocarbon adsorption is 2.28 kcal/mole. Desorption of isobutane as methane molecules is favored energetically as compared to desorption with an intact isobutane carbon skeleton (exchange reaction route).

The next step in the hydrogenolysis investigation is to catalyze the reaction by single crystal surfaces. There are no studies involving single crystal hydrogenolysis on iridium in the literature. This is the only way to isolate the most active surface. LEED and Auger spectroscopy can give additional information on surface geometry and composition under reaction conditions. This study can be complemented by a thermal desorption investigation.

Much more information is also needed on thin films. A question that needs to be answered is: "What is the effect of ambient gas exposure (H_2, O_2, hydrocarbon) during deposition on film structure?" It may be possible to induce specific orientation in the film by appropriate choice of deposition conditions.

Electron microscope, Auger spectroscopy and ESCA studies are a few suggestions for thin film analysis. Thermal desorption can also be used to give activation energies as a function of surface coverage. This would give some insight into surface heterogeneity.

REFERENCES

1. Morikawa, K., Benedict, W. S., and Taylor, H. S., J.A.C.S. 58, 1795 (1936).

2. Morikawa, K., Trenner, N. R., and Taylor, H. S., J.A.C.S. 59, 1103 (1937).

3. Cimino, A., Boudart, M., and Taylor, H. S., J. Phys. Chem. 58, 796 (1954).

4. Flinn, R. A., Larson, O. A., and Beuther, H., Ind. Eng. Chem. 52, 153 (1960).

5. Coonrad, H. L., Craptta, F. G., Garwood, W. E., Leaman, W. K., and Miale, J. J., Ind. Eng. Chem. 53, 727 (1961).

6. Archibald, R. C., Greensfelder, B. S., Halzman, G. and Rowie, D. H., Ind. Eng. Chem. 52, 745 (1960).

7. Sinfelt, J. H., Hurwitz, H., and Rahrer, J. C., J. Phys. Chem. 64, 892 (1960).

8. Sinfelt, J. H., A. Advan. Chem. Eng. 5, 37 (1964); J. Catalysis Science and Technology VI, (1981).

9. U.S. Patent 3,853,368 (1976).

10. Rasser, J. C., "Pt-Ir Reforming Catalysts," Delft University Press, Delft (1977).

11. Cook, G. A., "Survey of Modern Industrial Chemistry," Ann Arbor, Michigan Science Publishers, Inc. (1972).

12. Chem. Eng. News. July 3 (1972) Pg. 19.

13. Bond, G. C., "Catalysis by Metals," Academic Press New York (1962).

14. Ibach, H. and Lehwald, S., J. Vac. Sci. Technol. 15(2), 407 (1978).

15. Kesmodel, L. L., DuBois, L. H. and Somorjai, G. A., Chem. Phys. Lett. 56, 267 (1978).

16. Hansen, R. S., Arthur, J. R., Mimeault, V. J. and Rye, R. R., J. Phys. Chem. 70, 2787 (1966).

17. Wright, P. G., Ashmore, P. G. and Kemball, C., Trans. Faraday Soc. 54, 1692 (1958).

18. Dowie, R. W., Kemball, F. R. S., Kempling, J. C. and Whan, P. A., Proc. Roy. Soc. (Lond) A325, 491 (1972).

19. Sinfelt, J. H., and Yates, D. J. C., J. Catal. 8, 82 (1967).

20. Roberts, R. W., J. Phys. Chem. 68, 2718 (1964).

21. Sinfelt, J. H., Cat. Rev. 3, 175 (1970).

22. Mahaffy, P. and Hansen, R. S., J. Chem. Phys. 71(4), 1853 (1979).

23. Anderson, J. R., and Baker, B. G., Proc. Roy. Soc. (Lond) A271, 4026 (1963).

24. Boudart, M. and Ptak, L. D., J. Catal. 16, 90 (1970).

25. Anderson, J. R. and Avery, N. R., J. Catal. 446 (1966).

26. Anderson, J. R. and Avery, N. R., J. Catal. 7, 315 (1967).

27. Carter, S. L., Cusumano, J. A. and Sinfelt, J. H., J. Catal. 20, 1223 (1971).

28. Kinkade, N., Ph.D. thesis, Iowa State University.

29. Burron, Y., Maire, G., Muller, J. M. and Gault, F. G., J. Catal. 5, 428 (1966).

30. Rooney, J. J., J. Catal. 2, 53 (1963).

31. Sarkany, A. and Te'tengi, P., React. Kinet. Catal. Lett 12(3), 297 (1979).

32. Carter, J. L., Cusumano, J. A., and Sinfelt, J. H., J. Phys. Chem. 70(7), 2257 (1966).

33. Nieuwenhuys, B. E., Hagen, D. I., Rovida, G. and Somorjai, G. A., Surf. Sci. 59, 155 (1976).

34. Wittrig, T. S., Szvromi, P. D. and Weinberg, W. H., Surf. Sci. 6, 414 (1982).

35. Anderson, J. R., Advan. Cat. 23, 63 (1973).

36. Kempling, J. C. and Anderson, R. B., Ind. Eng. Chem. Process Res. and Develop., 11(1), 146 (1972).

37. Dushman, S., Scientific Foundations of Vacuum Technique, John Wiley and Sons, Inc. (1962).

38. Nieuwenhuys, B. E. and Somorjai, G. A. Surf. Sci. 72, 8 (1978).

39. Wittrig, T. S., Szuromi, P. D., Weinberg, W. H. J. Chem. Phys. 76, 3305 (1982).

40. Lang, B., Jagner, R. W., and Somorjai, G. A. Surf. Sci. 116, 414 (1982).

41. Christmann, K., Ertl, G., and Pignet, T. Surf. Sci. 54, 365 (1972).

42. Gudkov, B. S., Guczi, L., and Tetenyi, P. J. Cat. 74, 207 (1982).

43. Martin, G. A. J. Cat. 60, 345 (1979).

44. Heyward, D. O. and Trapnell, B. M. N. Chemisorption, Washington Butterworth (1964).

45. Chan, C. M. Cunningham, S. L., Luke, K. L., and Weinberg, W. H. Surf. Ci. 78, 15 (1978).

46. Chan, C. M., Van Hove, M. A., Weinberg, W. H., and Williams, E. D. Sollid State Com. 30, 47 (1979).

47. Chan, C. M., Cunningham, S. L., Van Hove, M. A., Weinberg, W. H., and Withrow, S. P. Surf. Sci. 67, 1 (1977).

48. Derochette, J. M. Surf. Sci. 118, 145 (1982).

49. Hagen, D. I., Nieuwenhuys, B. E., Rovida, G., and Somorjai, G. A. Surf. Sci. 57, 632 (1976).

50. Law, G. H. and Chitwood, H. C. U.S. Patent 2279469 to Union Carbide and Carbon Chemicals Company.

APPENDIX

Methane Desorption at 209°C

Hydrogen pressure = .45 torr isobutane pressure (torr)	Molecules of CH_4 desorbed x 10^{-16}
.03	2.61
.04	5.21
.06	11.17
.10	14.90
.13	15.64
.21	19.37
.25	19.37
.31	19.37
.38	20.86

Methane Desorption at 209°C

Isobutane pressure = .16 torr hydrogen pressure (torr)	Molecules of CH_4 desorbed x 10^{-16}
.04	18.62
.12	10.43
.21	8.19
.32	7.45
.42	5.96
.64	5.96
.77	5.21

Isobutane Order Plots at 209°C

Hydrogen pressure = .45 torr

Isobutane pressure (torr)	Rate (molecules/site·sec)	$\frac{\text{Isobutane pressure}}{\text{rate}}^{\frac{1}{2}}$
.01	1.34×10^{-4}	10.22
.03	2.07×10^{-4}	12.03
.04	2.32×10^{-4}	13.29
.07	2.52×10^{-4}	16.18
.11	2.46×10^{-4}	20.85
.12	2.41×10^{-4}	21.84
.13	2.12×10^{-4}	25.23
.15	2.12×10^{-4}	26.42
.18	2.12×10^{-4}	29.54
.25	1.97×10^{-4}	35.41
.38	1.44×10^{-4}	51.01
.49	1.12×10^{-4}	66.21

Hydrogen pressure = 2.03 torr

Isobutane pressure (torr)	Rate (molecules/site sec)	$\frac{\text{Isobutane pressure}}{\text{rate}}^{\frac{1}{2}}$
.09	$.32 \times 10^{-3}$	16.67
.12	$.43 \times 10^{-3}$	16.84
.16	$.74 \times 10^{-3}$	14.93
.25	$.86 \times 10^{-3}$	17.02
.33	$.98 \times 10^{-3}$	18.34
.41	$.94 \times 10^{-3}$	20.91
.67	$.88 \times 10^{-3}$	27.53
.89	$.67 \times 10^{-3}$	36.53
1.22	$.50 \times 10^{-3}$	49.42

Hydrogen pressure = 4.20 torr

Isobutane pressure (torr)	Rate (molecules/site·sec)	$\frac{\text{Isobutane pressure}^{\frac{1}{2}}}{\text{rate}}$
.09	$.46 \times 10^{-3}$	14.37
.27	1.08×10^{-3}	15.75
.67	1.80×10^{-3}	19.30
1.44	2.13×10^{-3}	26.04
1.76	1.80×10^{-3}	34.12
2.71	1.51×10^{-3}	53.18
4.01	$.96 \times 10^{-3}$	64.61

$$I = \frac{B}{A^{\frac{1}{2}}} P_{H_2}^{\frac{1}{2}} + \frac{1}{A^{\frac{1}{2}}}$$

P_{H_2} (torr)	$P_{H_2}^{\frac{1}{2}}$ ($torr^{\frac{1}{2}}$)	I ($torr^{\frac{1}{2}}$/(molecules/site·sec)$^{\frac{1}{2}}$)
.45	.67	8.59
2.03	1.43	10.68
4.20	2.05	11.12

$$S P_{H_2}^{\frac{1}{2}} = \frac{D}{A^{\frac{1}{2}}} P_{H_2}^{-\frac{1}{2}} + \frac{C}{A^{\frac{1}{2}}}$$

P_{H_2} (torr)	$P_{H_2}^{-\frac{1}{2}}$ ($torr^{-\frac{1}{2}}$)	$S P_{H_2}^{\frac{1}{2}}$ (torr/(molecules/site·sec)$^{\frac{1}{2}}$)
.45	1.49	77.28
2.03	.70	41.95
4.20	.49	27.94

Hydrogen Order Plot

at 209°C

Isobutane pressure = .04 torr

Hydrogen pressure (torr)	Rate (molecules/site·sec)
.04	$.16 \times 10^{-4}$
.09	$.56 \times 10^{-4}$
.09	$.56 \times 10^{-4}$
.14	$.70 \times 10^{-4}$
.21	$.84 \times 10^{-4}$
.41	2.19×10^{-4}
1.24	3.18×10^{-4}
1.98	3.21×10^{-4}
2.74	3.08×10^{-4}
3.27	2.90×10^{-4}
4.24	2.79×10^{-4}

Energy of Activation Data

Hydrogen pressure = .42 torr

Isobutane pressure = .17 torr

T(K)	Rate (molecules/site·sec)
449	2.12×10^{-4}
454	4.44×10^{-4}
468	10.08×10^{-4}
478	12.11×10^{-4}
494	26.63×10^{-4}
505	52.47×10^{-4}

Methane Desorbed as a Function of Temperature

T(K)	CH_4 (molecules x 10^{-16})
449	5.96
468	9.54
478	16.64
494	35.74
505	52.44

Methane Desorption at 175°C

Isobutane pressure = .16 torr

Hydrogen pressure (torr)	CH_4 desorbed (molecules x 10^{-16})
.04	6.70
.09	4.47
.09	5.62
.14	4.10
.21	2.98
.41	1.49
1.24	2.23
1.98	1.86
2.74	1.12
3.27	.74
4.24	.74

Methane Desorption at 175°C

Hydrogen pressure = .41 torr

Isobutane pressure (torr)	CH_4 desorbed (molecules x 10^{-16})
.04	.37
.07	.74
.08	1.49
.13	1.86
.16	2.23
.53	4.47
.92	6.70
1.22	6.70
2.08	6.70
2.87	6.70

Isobutane Order Plot at 175°C

Hydrogen pressure = 4.1 torr

Isobutane pressure (torr)	Rate (molecules/site·sec)	$\frac{\text{Iosbutane pressure}^{\frac{1}{2}}}{\text{rate}}$
.40	1.42×10^{-4}	50.31
.69	1.99×10^{-4}	55.87
.83	2.51×10^{-4}	54.55
1.34	3.50×10^{-4}	55.63
1.63	4.20×10^{-4}	59.14
5.29	4.19×10^{-4}	106.68
9.23	5.87×10^{-4}	146.68
12.21	3.46×10^{-4}	179.01
20.85	2.31×10^{-4}	285.38
28.78	1.53×10^{-4}	411.02

Hydrogen Order Plot

at 175°C

Isobutane pressure = 1.1 torr

Hydrogen pressure (torr)	Rate (molecules/site·sec)
.50	$.71 \times 10^{-4}$
.64	1.12×10^{-4}
1.11	2.33×10^{-4}
2.07	3.42×10^{-4}
3.30	4.08×10^{-4}
4.26	4.22×10^{-4}
6.03	3.66×10^{-4}
8.84	3.33×10^{-4}